

Unruh quantum Otto engine in the presence of a reflecting boundary

Arnab Mukherjee,^{a,1} Sunandan Gangopadhyay,^b A. S. Majumdar^c

S.N. Bose National Centre for Basic Sciences, JD Block, Sector-III, Salt Lake, Kolkata 700106, India

E-mail: arnab.mukherjee@bose.res.in,

sunandan.gangopadhyay@bose.res.in, archan@bose.res.in

ABSTRACT: We introduce a new model of relativistic quantum analogue of the classical Otto engine in the presence of a perfectly reflecting boundary. A single qubit acts as the working substance interacting with a massless quantum scalar field, with the boundary obeying the Dirichlet condition. The quantum vacuum serves as a thermal bath through the Unruh effect. We observe that the response function of the qubit gets significantly modified by the presence of the reflecting boundary. From the structure of the correlation function, we find that three different cases emerge, namely, the intermediate boundary regime, the near boundary regime, and the far boundary regime. As expected, the correlation in the far boundary regime approaches that of the Unruh quantum Otto engine (UQOE) when the reflecting boundary goes to infinity. The effect of the reflecting boundary is manifested through the reduction of the critical excitation probability of the qubit and the work output of the engine. In spite of the reduced work output, the efficiency of the engine remains unaltered even in the presence of the boundary.

¹Corresponding author.

Contents

1	Introduction	1
2	Quantum Otto cycle	3
3	Unruh quantum Otto engine in the presence of a reflecting boundary	5
4	Qubit-vacuum interaction	7
4.1	Evolution of the qubit	7
5	Vacuum correlation function	9
6	Evaluation of the response function	10
6.1	Evaluation of transition probability	12
6.1.1	Calculation of $\mathcal{F}_1(\mu, \nu)$	12
6.1.2	Calculation of $\mathcal{F}_2(\mu, \nu)$	14
6.2	Evaluation of transition probability in the near boundary regime	16
6.3	Evaluation of transition probability in the far boundary regime	17
7	Analysis of thermodynamical steps	17
7.1	Adiabatic expansion	18
7.2	Contact with the hot vacuum	18
7.3	Adiabatic contraction	19
7.4	Contact with the cold vacuum	19
7.5	Completing the cycle	19
8	Results	20
8.1	Demarcation of regimes with respect to the parameters	20
8.2	Transition probability	21
8.3	Work output in the presence of a reflecting boundary	24
9	Conclusions	27

1 Introduction

In recent years there has been an upsurge in interest in a field known as quantum thermodynamics which makes a connection between two fundamental physical theories, namely quantum mechanics and thermodynamics [1–4]. A long standing question that exists is whether it is possible to derive the laws of thermodynamics from quantum principles. This has made quantum thermodynamics an active area of research [5, 6]. Extensive studies

on heat engines treated quantum mechanically [7–19], have led to remarkable results and insights. By considering two level quantum systems, quantum versions of classical thermodynamic cycles have been proposed [20–24]. These are mainly quantum generalisations of the classical prototype of combustion engines.

Studies on quantum analogues of classical heat engines have gained importance from the perspective of gravitational physics. Connections between relativistic quantum mechanics, thermodynamics and black hole physics has already been established in some seminal works [25–29]. Therefore, it is quite natural to include relativistic notions in the domain of quantum thermodynamics. Relativistic extensions of quantum thermodynamic engines have been carried out in [30–33].

Investigations on field theoretic and relativistic phenomena in the presence of static or accelerating reflecting boundaries is an emerging topic in recent times. Accelerating mirrors can be considered as an analogue of the dynamical Casimir effect in (1+1) dimensions [34, 35], a prototype for black hole evaporation [36–40]. It has been observed that there is a strong connection between accelerating mirrors and black hole physics [41–44].

Innovation in nanofabrication techniques [45, 46] have enhanced the scope of experimental realization of atomic excitations in nanoscale waveguides [47], through trapped atoms in optical nanofibers [48, 49]. These avenues open up the possibilities of exploration of fundamental quantum optical aspects like atom-photon lattices [50]. Studies on relativistic quantum phenomena in superconducting circuits [51, 52], and secure quantum communication over long-distances [53–56], show the importance of reflecting boundaries which also play significant physical role in the context of atom-field interaction [57, 58], holographic entanglement entropy [59], and quantum entanglement [60–63].

Motivated by the importance of the reflecting boundary in the context of superconducting circuits, quantum communication, atom-field interaction and quantum entanglement, in this paper we aim to investigate the effect of a reflecting boundary in case of quantum heat engines. To begin this investigation, at first we introduce a new model for the relativistic quantum analogue of the classical Otto engine [64–68]. Here we consider a single qubit (Unruh-DeWitt detector) acting as the working substance, interacting linearly with a massless quantum scalar field in the presence of a perfectly reflecting boundary which obeys the Dirichlet boundary condition. The quantum vacuum serves as a thermal bath through the Unruh effect [29].

The importance of carrying out this investigation in the presence of a reflecting boundary lies in its relevance to cavity quantum electrodynamics which is a thrust area of fundamental research and has practical applications [69]. In particular, techniques of quantum electrodynamics in a cavity can be applied to investigate the Unruh-Davies effect inside cavities [70, 71]. Cavity quantum electrodynamical setups are also important in superconducting circuits which can implement large acceleration [52]. The presence of boundaries have also been incorporated in theoretical investigations of radiative processes of entangled atoms [72].

One can understand the effect of the reflecting boundary from two perspectives. From a physical point of view, Poincare symmetry is broken by the presence of the boundary and thus, spectral density of the field is also modified, which accordingly alters the dynamics

of the detector-field system [61]. On the other hand, from another technical viewpoint, exploiting the symmetry in the model, one can solve the problem of the qubit interacting with a boundary modified field by using the method of image charge problem. It is well known that the correlation function between the scalar fields commonly known as the Wightman function gets significantly modified by the presence of the reflecting boundary [73].

Since the response function of the qubit only depends on this correlation function of the scalar field [74–77], so boundary effects must be captured in the response function of the qubit. The presence of reflecting boundary affects the quantum fields [78], the correlation function between the fields and the rate of spontaneous emission of excited atoms [79]. Therefore, one would expect modifications in the response function and transition probability of the qubit.

In the present work we explore how such modifications in the response function affect the transition probability and the amount of work extraction from the quantum vacuum fluctuation of the massless scalar field. We choose the system parameters in the range of current experimntal values in domain of superconducting circuits where large atomic acceleration can be realized [80]. Based on such a parameter range, it is possible to demarcate three different regimes, namely, the near boundary regime, the intermediate boundary regime, and the far boundary regime, as we show in our analysis. We study the behaviour of the above observable quantities in each case as a function of the qubit acceleration, as well as the initial qubit state parameters, and the bath temperatures. We observe several interesting variations in the observable properties corresponding to the three different regimes. We find that though the reflecting boundary adversely impacts the work output, the efficiency of the heat engine remains unaltered.

The paper is organised as follows. In section 2, we recapitulate certain basic definitions of quantum thermodynamics and quantum Otto cycles. In section 3, a new form of relativistic extension of the quantum Otto cycle is introduced. Sections 4 and 5 are devoted to study how a qubit interacts with the quantum vacuum leading to the modification of the correlation function in the presence of the reflecting boundary. In section 6, the response function, which is a key factor for calculating the transition probability, is evaluated. In section 7 the thermodynamical analysis of the heat engine is performed. Section 8 contains a detailed analysis of the effects due to the reflecting boundary on the transition probability, work output and efficiency. Finally, we conclude in section 9.

2 Quantum Otto cycle

Thermodynamic cycles provide foundational working principles of the heat engines [81]. To begin our discussion, we start by reviewing the basic features of the quantum otto cycle (QOC). In the quantum counterpart of the classical Otto cycle for a qubit [20, 21] the energy gap between the two levels are not fixed and can be adjusted by an external (weak electric or magnetic) stimulation without hampering the state of the system. Considering a qubit having a ground state $|g\rangle$, and an excited state $|e\rangle$, described by a density matrix $\rho(t)$ and associated time dependent Hamiltonian $\mathcal{H}(t)$, the average energy of the system

$\langle E(t) \rangle = \text{Tr}[\rho(t)\mathcal{H}(t)]$ satisfies the following equation [82]

$$\partial_t \langle E(t) \rangle = \text{Tr}[\partial_t \rho(t)\mathcal{H}(t)] + \text{Tr}[\rho(t)\partial_t \mathcal{H}(t)] . \quad (2.1)$$

This equation is identical with the first law thermodynamics and can be treated as its quantum version where the first term and second term on the right hand side can be described as the change in the internal state and population of the system and the external shifting of the energy levels of the system, respectively. Therefore, the following identifications can be made

$$\langle Q \rangle = \int_0^{\mathcal{T}} dt \text{Tr} \left[\frac{\partial \rho(t)}{\partial t} \mathcal{H}(t) \right] \quad (2.2)$$

$$\langle W \rangle = \int_0^{\mathcal{T}} dt \text{Tr} \left[\rho(t) \frac{\partial \mathcal{H}(t)}{\partial t} \right] \quad (2.3)$$

where $\langle Q \rangle$ is the average heat transfer to the system and $\langle W \rangle$ is the work done on the system over the interaction time \mathcal{T} .

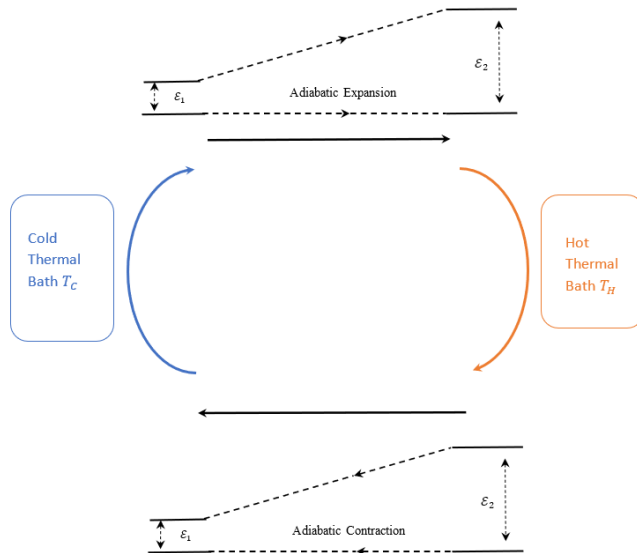


Figure 1: Thermodynamic cycle of Quantum Otto Engine.

Considering the ground state and excited state energy of the qubit being zero and \mathcal{E}_1 respectively, the Hamiltonian of the qubit turns out to be $H = \mathcal{E}_1|e\rangle\langle e|$. We also consider that the Otto cycle begins with the system in an initial state $\rho_0 = p|e\rangle\langle e| + (1-p)|g\rangle\langle g|$. Thermodynamical steps of the QOC are as follows

1. In the first step, without changing form of the initial state the system undergoes an adiabatic expansion of the energy gap \mathcal{E}_1 to \mathcal{E}_2 . In this step, there is no heat exchange with the environment but some work is done.
2. In the second step, the qubit ρ_0 is attached with a thermal bath at temperature T_H . After the interaction for the time \mathcal{T}_2 , heat is exchanged and the initial state of the

system is changed to, $\rho = (p + \delta p_H)|e\rangle\langle e| + (1 - p - \delta p_H)|g\rangle\langle g|$ where δp_H is the transition probability between two levels of the qubit due to the first interaction with the thermal bath. In this step, the total amount of work done is zero.

3. In the third step, keeping the state fixed at ρ the system undergoes an adiabatic compression and the energy level of the qubit is reduced from \mathcal{E}_2 to \mathcal{E}_1 . In this step also, no heat is exchanged with the environment but a sufficient amount of work is done. This is the power stroke of the cycle where the system performs work.
4. In the final step, the system is attached with a thermal bath having a lesser temperature compared to that of the previous bath, $T_C < T_H$. After interaction time \mathcal{T}_1 , the final state of the qubit becomes $\rho_f = (p + \delta p_H + \delta p_C)|e\rangle\langle e| + (1 - p - \delta p_H - \delta p_C)|g\rangle\langle g|$, where δp_C is the transition probability between two levels of the qubit due to the second interaction with the thermal bath. In this step also, no work is done.

For completing the cycle, we must have $\delta p_H + \delta p_C = 0$. It is worth noting here that using the von Neumann entropy $S = -k_B \text{Tr}[\rho \log \rho]$ and the equilibrium Boltzmann distribution $\rho = \exp(-\beta \mathcal{H})/Z$ where Z is the partition function, one can show that $T\delta S = \text{Tr}[\delta \rho \mathcal{H}] = \delta Q$, which shows the compatibility of the quantum thermodynamics domain with the usual classical thermodynamics.

3 Unruh quantum Otto engine in the presence of a reflecting boundary

Extension of the quantum Otto engine (QOE) to the relativistic domain has been made earlier by exploiting the notion of Unruh effect [64]. Here our aim is to see that how a Unruh quantum Otto engine (UQOE) behaves in the presence of a reflecting boundary. To address this point, we introduce a single perfectly reflecting boundary. Consider that the qubit is at a distance of z_0 from the boundary and accelerates along the x direction as depicted in Figure 2b.

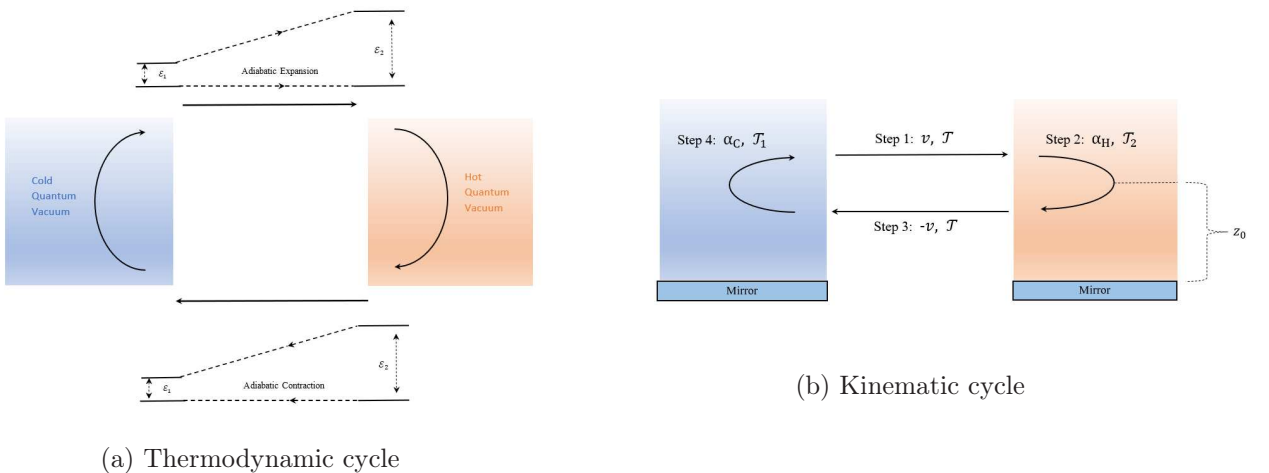


Figure 2: Different cycles of UQOE with a single reflecting boundary.

From the thermodynamical cycle of UQOE in the presence of a single reflecting boundary (Figure 2a), steps 2 and 4 of the QOC cold and hot temperatures will correspond to different accelerations α_H and α_C . As the temperature of the vacuum is proportional of the particle's acceleration, we must have $\alpha_H > \alpha_C$ for one vacuum to have higher temperature than the other, i.e., $T_H > T_C$, and thus transfer work from the vacuum to the system. We will assume in the other two steps (step 1 and step 3) that the qubit travels at constant velocity and can be isolated from the quantum field vacuum. Apart from this we also require that the kinematic cycle of the qubit (Figure 2b) is closed. Steps of the kinematic cycle of UQOE with a single reflecting boundary are as follows.

1. The qubit moves at constant velocity v for time \mathcal{T} , during which the energy gap expands from \mathcal{E}_1 to \mathcal{E}_2 . This step is similar to the adiabatic expansion.
2. In this step, the qubit undergoes a constant acceleration α_H over the interaction time \mathcal{T}_2 . During this interaction velocity of the qubit changes from v to $-v$ and the quantum vacuum acts as a hot thermal reservoir.
3. The qubit moves at constant velocity $-v$ for time \mathcal{T} , during which the energy gap reduces from \mathcal{E}_2 to \mathcal{E}_1 . This step is similar to the adiabatic contraction.
4. In this step, the qubit undergoes a constant acceleration α_C over the interaction time \mathcal{T}_1 . During this interaction the quantum vacuum serves as a cold thermal reservoir. The velocity of the qubit changes from $-v$ to v and it returns to its initial state.

Here \mathcal{T}_1 and \mathcal{T}_2 are the time in which the qubit accelerates and interacts with the quantum vacuum (the velocity of the qubit changes from v to $-v$, and $-v$ to v , respectively). For closing the kinematical cycle and returning the qubit to its original state, \mathcal{T}_1 and \mathcal{T}_2 must have some fixed value.

In the relativistic picture it is well known that a constantly accelerated observer moving with a proper acceleration α in proper time τ has a hyperbolic worldline $x^\mu(\tau) = (t(\tau), \mathbf{x}(\tau))$ where

$$t(\tau) = \frac{c}{\alpha} \sinh\left(\frac{\alpha\tau}{c}\right) \quad x(\tau) = \frac{c^2}{\alpha} \cosh\left(\frac{\alpha\tau}{c}\right). \quad (3.1)$$

considering above worldline for a qubit, the qubit velocity v turns out to be

$$v = c \tanh\left(\frac{\alpha\tau}{c}\right) \quad (3.2)$$

Therefore, the time taken by the qubit to reach the velocity v from $\tau = 0$ is

$$\tau = \frac{c}{\alpha} \tanh^{-1}\left(\frac{v}{c}\right) = \frac{c}{\alpha} \tanh^{-1}(\beta) \quad (3.3)$$

Now, if we consider that at time $t = -\tau$ and $t = \tau$ the velocity of the qubit is $-v$ and v respectively, then it takes the time $2\tau = \frac{2c}{\alpha} \tanh^{-1}(\beta)$ to change the velocity from $-v$ to v with a constant acceleration α . Hence, in second and fourth step in the thermodynamic as

well as the kinematic cycle, the qubit must accelerate for the following times

$$\mathcal{T}_2 = \frac{2c}{\alpha_H} \tanh^{-1}(\beta) \quad (3.4)$$

$$\mathcal{T}_1 = \frac{2c}{\alpha_C} \tanh^{-1}(\beta) \quad (3.5)$$

with accelerations α_H and α_C , respectively. From here we can conclude that the vacuum behaves as a hot or cold reservoir over these amounts of finite interaction times.

4 Qubit-vacuum interaction

We consider a qubit interacting with a real massless scalar field $\phi[x(\tau)]$ linearly, in the presence of a reflecting boundary where the distance between the qubit and the boundary is z_0 . The Hamiltonian that describes the qubit-field interacting system in the instantaneous inertial frame of the qubit reads [73]

$$\mathcal{H} = \mathcal{H}_{qubit} + \mathcal{H}_{field} + \mathcal{H}_{int} \quad (4.1)$$

where

$$\mathcal{H}_{qubit} = \mathcal{E}|e\rangle\langle e| \quad (4.2)$$

$$\mathcal{H}_{field} = \int d^3k \mathcal{E}(k) b^\dagger(\mathbf{k})b(\mathbf{k}) \quad (4.3)$$

$$\mathcal{H}_{int} = \lambda m(\tau) \phi[x(\tau)]. \quad (4.4)$$

Here $b(\mathbf{k})$ and $b^\dagger(\mathbf{k})$ are the bosonic operators of the scalar field [83], λ is a weak qubit field coupling constant having the dimension $[M^{3/2}L^{5/2}T^{-1}]$ and $m(\tau)$ is the monopole operator of the qubit. It may be noted that in this model we consider that the qubit acts as a point particle and the total Hamiltonian of the system is written in the interaction picture so that we can use the free mode expansion of the massless scalar field $\phi[x(\tau)]$. The monopole operator $m(\tau)$ can be written in this picture as

$$m(\tau) = e^{+\frac{i\mathcal{E}\tau}{\hbar}}|e\rangle\langle g| + e^{-\frac{i\mathcal{E}\tau}{\hbar}}|g\rangle\langle e| = \begin{pmatrix} 0 & e^{+i\mathcal{E}\tau/\hbar} \\ e^{-i\mathcal{E}\tau/\hbar} & 0 \end{pmatrix}. \quad (4.5)$$

4.1 Evolution of the qubit

Let us consider that the initial density matrix of the qubit is given by

$$\rho_0 = p|e\rangle\langle e| + (1-p)|g\rangle\langle g| = \begin{pmatrix} p & 0 \\ 0 & 1-p \end{pmatrix} \quad (4.6)$$

where p is the probability for the qubit remaining in the excited state. In an inertial frame, the initial density matrix of the scalar field having the vacuum state $|0\rangle$ is given by

$$\rho_{field} = |0\rangle\langle 0|. \quad (4.7)$$

Therefore, the initial state of the interaction between qubit and the quantum vacuum can be taken as

$$\varrho_0 = \rho_0 \otimes \rho_{field} . \quad (4.8)$$

Now, using the time evolution operator $U_{\mathcal{T}}$, we can write down the density matrix of the interaction over a period \mathcal{T} as

$$\varrho_{\mathcal{T}} = U_{\mathcal{T}} \varrho_0 U_{\mathcal{T}}^\dagger . \quad (4.9)$$

The time evolution operator $U_{\mathcal{T}}$ satisfies the evolution equation

$$i\hbar \frac{\partial U_{\mathcal{T}}}{\partial \tau} = \mathcal{H}_{int}(\tau) U_{\mathcal{T}} \quad (4.10)$$

whose solution is given by the Dyson series [83]

$$U_{\mathcal{T}} = \mathbf{1} - \frac{i}{\hbar} \int_{t_0}^t d\tau \mathcal{H}_{int}(\tau) - \frac{1}{2\hbar^2} \int_{t_0}^t d\tau \int_{t_0}^t d\tau' \hat{T}\{\mathcal{H}_{int}(\tau) \mathcal{H}_{int}(\tau')\} + \mathcal{O}(\lambda^3) \quad (4.11)$$

where \hat{T} is the time ordering operator defined as

$$\hat{T}\{A(t)B(t')\} = \Theta(t-t')A(t)B(t') + \Theta(t'-t)B(t')A(t). \quad (4.12)$$

Substituting eq.(4.11) into eq.(4.9), we get

$$\varrho_{\mathcal{T}} = \varrho_0 - \frac{i}{\hbar} \int_{t_0}^t d\tau [\mathcal{H}_{int}(\tau), \varrho_0] - \frac{1}{2\hbar^2} \int_{t_0}^t d\tau \int_{t_0}^t d\tau' \hat{T}\{[\mathcal{H}_{int}(\tau), [\mathcal{H}_{int}(\tau'), \varrho_0]]\} + \mathcal{O}(\lambda^3). \quad (4.13)$$

Our primary concern is the evolution of the qubit in the interaction picture. As we are not interested about the evolution of the vacuum state, hence after taking a partial trace over the field degrees of freedom to extract the evolution of the qubit state, we get

$$\rho_{\mathcal{T}} = \text{Tr}_{\text{field}}[\varrho_{\mathcal{T}}] . \quad (4.14)$$

Calculating the partial trace in eq.(4.13) term by term, we see that the zeroth order term is simply the initial state of the qubit, the first order term vanishes as the vacuum expectation value of the field operator vanishes, while the second order term gives the main contribution to the evolving state. Hence, after the interaction time \mathcal{T} , the density matrix of the qubit becomes

$$\rho_{\mathcal{T}} = \begin{pmatrix} p + \delta p_{\mathcal{T}} & 0 \\ 0 & 1 - p - \delta p_{\mathcal{T}} \end{pmatrix} + \mathcal{O}(\lambda^4) \quad (4.15)$$

where $\delta p_{\mathcal{T}}$ is the transition probability between the levels of the qubit occurring due to quantum vacuum fluctuations. Therefore, transition probability can be recast as

$$\delta p_{\mathcal{T}} = \frac{\lambda^2}{\hbar^2} \int_{-\bar{t}}^t d\tau \int_{-\bar{t}}^t d\tau' ((1-p) e^{-i\mathcal{E}(\Delta\tau)/\hbar} - p e^{+i\mathcal{E}(\Delta\tau)/\hbar}) \mathcal{G}^+(\tau, \tau') \quad (4.16)$$

where $\mathcal{G}^+(\tau, \tau')$ is known as the positive frequency Wightman function [84] given by

$$\mathcal{G}^+(\tau, \tau') = \langle 0 | \phi[x(\tau)] \phi[x(\tau')] | 0 \rangle. \quad (4.17)$$

Introducing a switching function $\varpi_{\mathcal{T}}(\tau)$ and taking the Markovian approximation, eq.(4.16) becomes [64, 65]

$$\begin{aligned} \delta p_{\mathcal{T}} &= \frac{\lambda^2}{\hbar^2} \int_{-\infty}^{+\infty} d\tau \int_{-\infty}^{+\infty} d\tau' \varpi_{\mathcal{T}}(\tau) \varpi_{\mathcal{T}}(\tau') ((1-p) e^{-i\mathcal{E}(\Delta\tau)/\hbar} - p e^{+i\mathcal{E}(\Delta\tau)/\hbar}) \mathcal{G}^+(\tau, \tau') \\ &= \lambda^2 [(1-p) \mathcal{F}(\mathcal{E}, \mathcal{T}) - p \mathcal{F}(-\mathcal{E}, \mathcal{T})]. \end{aligned} \quad (4.18)$$

The response function of the qubit can be defined as

$$\mathcal{F}(\mathcal{E}, \mathcal{T}) = \frac{1}{\hbar^2} \int_{-\infty}^{+\infty} d\tau \int_{-\infty}^{+\infty} d\tau' \varpi_{\mathcal{T}}(\tau) \varpi_{\mathcal{T}}(\tau') \mathcal{G}^+(\tau, \tau') e^{-i\mathcal{E}(\Delta\tau)/\hbar}. \quad (4.19)$$

5 Vacuum correlation function

In the presence of a reflecting boundary, the Wightman function is the sum of the empty space part and a part that depends on the presence of the mirror [73]. We can write it as [84]

$$\mathcal{G}^+(\tau, \tau') = -\frac{\hbar}{4\pi^2 c} \left[\frac{1}{(c\Delta t - i\eta)^2 - (x-x')^2 - (y-y')^2 - (z-z')^2} - \frac{1}{(c\Delta t - i\eta)^2 - (x-x')^2 - (y-y')^2 - (z+z')^2} \right] \quad (5.1)$$

where Δt is the difference between qubit coordinates $t(\tau)$ at two different proper times and η is a small parameter. In the laboratory frame the trajectory of an uniformly accelerating qubit along the x direction at a distance z_0 from the reflecting boundary reads,

$$\begin{aligned} t(\tau) &= \frac{c}{\alpha} \sinh\left(\frac{\alpha\tau}{c}\right), & x(\tau) &= \frac{c^2}{\alpha} \cosh\left(\frac{\alpha\tau}{c}\right) \\ y(\tau) &= 0, & z(\tau) &= z_0. \end{aligned} \quad (5.2)$$

Here α is the proper acceleration and τ is the proper time of the qubit. Now, using eqs.(5.2), we get

$$\begin{aligned} c\Delta t &= c(t(\tau) - t(\tau')) \\ &= \frac{c^2}{\alpha} \left[\sinh\left(\frac{\alpha\tau}{c}\right) - \sinh\left(\frac{\alpha\tau'}{c}\right) \right]. \end{aligned} \quad (5.3)$$

Similarly, we also have the following relation

$$\Delta x = \frac{c^2}{\alpha} \left[\cosh\left(\frac{\alpha\tau}{c}\right) - \cosh\left(\frac{\alpha\tau'}{c}\right) \right], \quad \Delta y = 0, \quad \Delta z = 0. \quad (5.4)$$

Using the above two results and keeping terms upto $\mathcal{O}(\eta)$, we get

$$\begin{aligned}
(c\Delta t - i\eta)^2 - (\Delta x)^2 &= \left[\frac{c^2}{\alpha} \left\{ \sinh\left(\frac{\alpha\tau}{c}\right) - \sinh\left(\frac{\alpha\tau'}{c}\right) \right\} - i\eta \right]^2 - \left[\frac{c^2}{\alpha} \left\{ \cosh\left(\frac{\alpha\tau}{c}\right) - \cosh\left(\frac{\alpha\tau'}{c}\right) \right\} \right]^2 \\
&= -\frac{2c^4}{\alpha^2} + \frac{2c^4}{\alpha^2} \left\{ \cosh\left(\frac{\alpha\tau}{c}\right) \cosh\left(\frac{\alpha\tau'}{c}\right) - \sinh\left(\frac{\alpha\tau}{c}\right) \sinh\left(\frac{\alpha\tau'}{c}\right) \right\} - i\eta \\
&= -\frac{2c^4}{\alpha^2} + \frac{2c^4}{\alpha^2} \left\{ \cosh\left(\frac{\alpha(\Delta\tau)}{c}\right) - i\eta \right\} \\
&= -\frac{2c^4}{\alpha^2} \left[1 - \cosh\left(\frac{\alpha(\Delta\tau)}{c}\right) - i\eta \right] \\
&= \frac{4c^4}{\alpha^2} \sinh^2\left(\frac{\alpha(\Delta\tau)}{2c} - i\eta\right)
\end{aligned} \tag{5.5}$$

where $\Delta\tau$ is the difference between two different proper times τ and τ' . In a similar way, it can be shown that

$$(c\Delta t - i\eta)^2 - (x - x')^2 - (y - y')^2 - (z + z')^2 = \frac{4c^4}{\alpha^2} \left[\sinh^2\left(\frac{\alpha(\Delta\tau)}{2c} - i\eta\right) - \frac{z_0^2\alpha^2}{c^4} \right]. \tag{5.6}$$

Therefore, after using eq.(s)(5.5, 5.6) in eq.(5.1), the Wightman function in the presence of a reflecting boundary takes the form

$$\mathcal{G}^+(\tau, \tau') = -\frac{\hbar\alpha^2}{16\pi^2c^5} \left[\frac{1}{\sinh^2\left(\frac{\alpha(\Delta\tau)}{2c} - i\eta\right)} - \frac{1}{\sinh^2\left(\frac{\alpha(\Delta\tau)}{2c} - i\eta\right) - \frac{z_0^2\alpha^2}{c^4}} \right]. \tag{5.7}$$

6 Evaluation of the response function

In this section, we proceed to calculate the response function. From the time evolution of the qubit eq.(4.18), the transition probability between the energy levels of the qubit can be written as

$$\delta p = \lambda^2[(1 - p)\mathcal{F}(\mathcal{E}, \mathcal{T}) - p\mathcal{F}(-\mathcal{E}, \mathcal{T})] \tag{6.1}$$

where

$$\mathcal{F}(\mathcal{E}, \mathcal{T}) = \frac{1}{\hbar^2} \int_{-\infty}^{+\infty} d\tau \int_{-\infty}^{+\infty} d\tau' \varpi_{\mathcal{T}}(\tau) \varpi_{\mathcal{T}}(\tau') \mathcal{G}^+(\tau, \tau') e^{-i\mathcal{E}(\Delta\tau)/\hbar}. \tag{6.2}$$

Following [64, 65], we now consider a Lorentzian switching function

$$\varpi_{\mathcal{T}}(\tau) = \frac{(\mathcal{T}/2)^2}{\tau^2 + (\mathcal{T}/2)^2}. \tag{6.3}$$

Changing the variables from $(\tau, \tau') \rightarrow (m, n)$ by the transformations $m = \tau - \tau'$ and $n = \tau + \tau'$, we can recast the above equation as

$$\mathcal{F}(\mathcal{E}, \mathcal{T}) = \frac{1}{2\hbar^2} \int_{-\infty}^{+\infty} dm \left(\mathcal{G}^+(\tau, \tau') e^{-i\mathcal{E}m/\hbar} \int_{-\infty}^{+\infty} dn \varpi_{\mathcal{T}}((m+n)/2) \varpi_{\mathcal{T}}((m-n)/2) \right). \tag{6.4}$$

The advantage of the Lorentzian regulator is that it enables us to extend the integration to the complex plane and use the residue theorem since $\varpi_{\mathcal{T}}(z) \rightarrow 0$ for $|z| \rightarrow \infty$ for all $z \in \mathbb{C}$. Putting eq.(6.3) in the integral containing switching functions, we get

$$\int_{-\infty}^{+\infty} dn \varpi_{\mathcal{T}}((m+n)/2) \varpi_{\mathcal{T}}((m-n)/2) = \int_{-\infty}^{+\infty} dn \frac{\mathcal{T}^4}{[(n+m)^2 + \mathcal{T}^2][(n-m)^2 + \mathcal{T}^2]} . \quad (6.5)$$

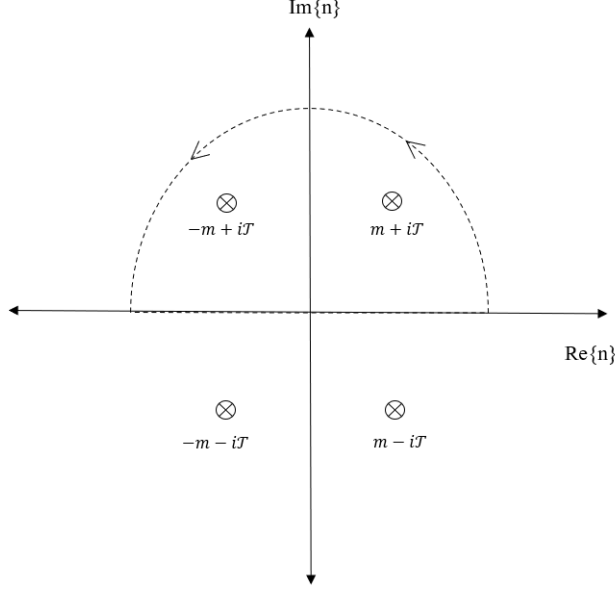


Figure 3: Pole structures of the integral (6.5).

The above integral can be evaluated by employing the method of contour integral [85]. Figure 3 shows the pole structure of eq.(6.5). Considering the contour in the upper half plane we see that the pole $n = m + iT$ and $n = -m + iT$ lies inside the contour. Therefore, residues at the point $n = m + iT$ and $n = -m + iT$ read

$$R_1 = \frac{\mathcal{T}^4}{8im\mathcal{T}(m + iT)} \quad (6.6)$$

$$R_2 = \frac{\mathcal{T}^4}{8im\mathcal{T}(m - iT)} . \quad (6.7)$$

Hence, we get

$$\begin{aligned} \int_{-\infty}^{+\infty} dn \frac{\mathcal{T}^4}{[(n+m)^2 + \mathcal{T}^2][(n-m)^2 + \mathcal{T}^2]} &= 2\pi i [R_1 + R_2] \\ &= 2\pi i \left[\frac{\mathcal{T}^4}{8im\mathcal{T}(m + iT)} + \frac{\mathcal{T}^4}{8im\mathcal{T}(m - iT)} \right] \\ &= \frac{\pi\mathcal{T}^3}{2} \frac{1}{(m^2 + \mathcal{T}^2)} . \end{aligned} \quad (6.8)$$

Using the result of the Lorentzian switching function integral eq.(6.8) in eq.(6.4), the response function simplifies to

$$\mathcal{F}(\mathcal{E}, \mathcal{T}) = \frac{\pi \mathcal{T}^3}{4\hbar^2} \int_{-\infty}^{+\infty} dm \frac{\mathcal{G}^+(\tau, \tau')}{m^2 + \mathcal{T}^2} e^{-i\mathcal{E}m/\hbar}. \quad (6.9)$$

Now, incorporating the Wightman function in the above equation, we can evaluate the response function for the following scenarios.

6.1 Evaluation of transition probability

Using eq.(5.7) in eq.(6.9), we have

$$\mathcal{F}(\mathcal{E}, \mathcal{T}) = \mathcal{F}_1(\mathcal{E}, \mathcal{T}) + \mathcal{F}_2(\mathcal{E}, \mathcal{T}) \quad (6.10)$$

where

$$\mathcal{F}_1(\mathcal{E}, \mathcal{T}) = -\frac{\pi \mathcal{T}^3}{4\hbar c} \frac{\alpha^2}{16\pi^2 c^4} \int_{-\infty}^{+\infty} dm \frac{e^{-i\mathcal{E}m/\hbar}}{m^2 + \mathcal{T}^2} \frac{1}{\sinh^2\left(\frac{\alpha m}{2c} - i\eta\right)} \quad (6.11)$$

$$\mathcal{F}_2(\mathcal{E}, \mathcal{T}) = \frac{\pi \mathcal{T}^3}{4\hbar c} \frac{\alpha^2}{16\pi^2 c^4} \int_{-\infty}^{+\infty} dm \frac{e^{-i\mathcal{E}m/\hbar}}{m^2 + \mathcal{T}^2} \frac{1}{\sinh^2\left(\frac{\alpha m}{2c} - i\eta\right) - \frac{z_0^2 \alpha^2}{c^4}}. \quad (6.12)$$

Defining dimensionless variables

$$\begin{aligned} z &= z_0 \alpha / c^2, & \mu &= \mathcal{E}c / (\hbar \alpha) \\ \nu &= \alpha \mathcal{T} / c, & \xi &= \alpha m / c \end{aligned} \quad (6.13)$$

and recasting the above integrals in terms of these dimensionless variables, we get

$$\mathcal{F}_1(\mu, \nu) = -\frac{\nu^3}{64\pi \hbar c^3} \int_{-\infty}^{+\infty} d\xi \frac{e^{-i\mu\xi}}{\xi^2 + \nu^2} \frac{1}{\sinh^2\left(\frac{\xi}{2} - i\eta\right)} \quad (6.14)$$

and

$$\mathcal{F}_2(\mu, \nu) = \frac{\nu^3}{64\pi \hbar c^3} \int_{-\infty}^{+\infty} d\xi \frac{e^{-i\mu\xi}}{\xi^2 + \nu^2} \frac{1}{\left[\sinh^2\left(\frac{\xi}{2} - i\eta\right) - z^2\right]}. \quad (6.15)$$

To carry out the integrals in eq(s). (6.14, 6.15), we use the method of contour integration.

6.1.1 Calculation of $\mathcal{F}_1(\mu, \nu)$

Using the series representation [86]

$$\operatorname{csch}^2\left[\frac{\xi}{2} - i\eta\right] = \sum_{k=-\infty}^{\infty} \frac{4}{(\xi - 2i\eta - 2i\pi k)^2} = \sum_{k=-\infty}^{\infty} \frac{4}{(\xi - i\epsilon - 2i\pi k)^2} \quad (6.16)$$

where $\epsilon = 2\eta$, in eq.(6.14), we get

$$\mathcal{F}_1(\mu, \nu) = \frac{1}{\hbar c^3} \left[\mathcal{I}_0 + \sum_{k=1}^{\infty} \mathcal{I}_k \right] \quad (6.17)$$

where I_0 and I_k are given by the integrals

$$\mathcal{I}_0 = -\frac{\nu^3}{16\pi} \int_{-\infty}^{+\infty} d\xi \frac{e^{-i\mu\xi}}{\xi^2 + \nu^2} \frac{1}{(\xi - i\epsilon)^2} \quad (6.18)$$

$$\mathcal{I}_k = -\frac{\nu^3}{16\pi} \int_{-\infty}^{+\infty} d\xi \frac{e^{-i\mu\xi}}{\xi^2 + \nu^2} \left\{ \frac{1}{(\xi - 2i\pi k)^2} + \frac{1}{(\xi + 2i\pi k)^2} \right\}. \quad (6.19)$$

For carrying out the integral \mathcal{I}_0 , we consider the range $\mu < 0$ and close the contour in the

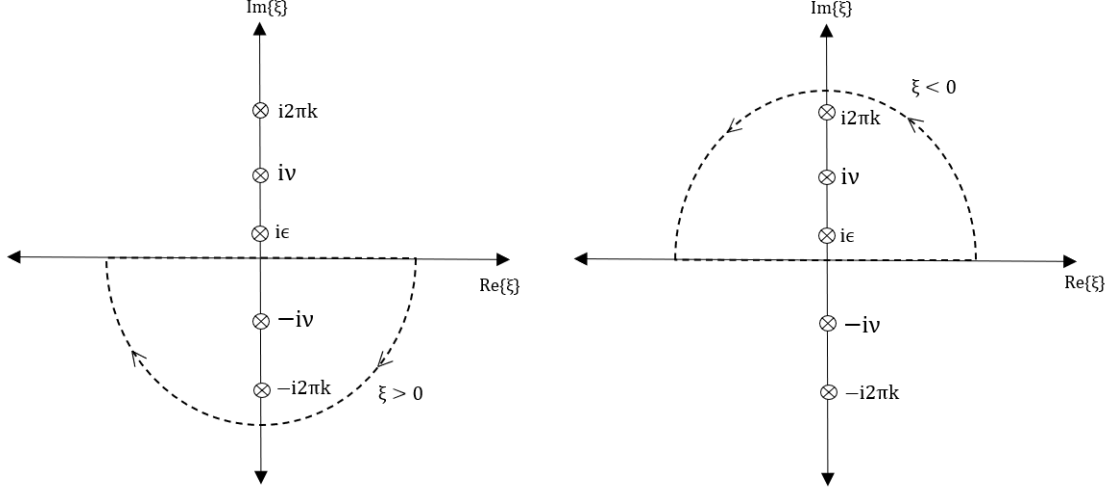


Figure 4: Pole structures of the integrals (6.18) and (6.19).

upper half plane and find one first order pole at $\xi = i\nu$ and one second order pole at $\xi = i\epsilon$. Calculating the residues for all poles and taking the limit $\epsilon \rightarrow 0$, we get

$$R_1 = -e^{\mu\nu}/(2i\nu^3), \quad R_2 = -i\mu/\nu^2. \quad (6.20)$$

Hence, we have

$$\begin{aligned} \mathcal{I}_0 &= -\frac{\nu^3}{16\pi} \left[2\pi i (R_1 + R_2) \right] \\ &= -\frac{\nu^3}{16\pi} \left[-\frac{\pi}{\nu^3} e^{\mu\nu} + 2\pi\mu \frac{1}{\nu^2} \right]. \end{aligned} \quad (6.21)$$

Similarly, when $\mu > 0$, the contour has to be closed in the lower half plane and ξ will only pick a first order pole at, $\xi = -i\nu$. Calculating the residue for the pole and taking the limit $\epsilon \rightarrow 0$, we get

$$R_3 = e^{-\mu\nu}/(2i\nu^3). \quad (6.22)$$

Hence,

$$\begin{aligned} \mathcal{I}_0 &= -\frac{\nu^3}{16\pi} \left[-2\pi i (R_3) \right] \\ &= -\frac{\nu^3}{16\pi} \left[\frac{\pi}{\nu^3} e^{\mu\nu} \right]. \end{aligned} \quad (6.23)$$

Therefore, considering both the region $\mu < 0$ and $\mu > 0$, we can write

$$\mathcal{I}_0 = \frac{1}{16} \left[e^{-|\mu|\nu} + 2|\mu|\nu\Theta(-\mu) \right] \quad (6.24)$$

with

$$\begin{aligned} \Theta(-\mu) &= 1, \quad \text{when } \mu < 0 \\ &= 0, \quad \text{otherwise.} \end{aligned}$$

We now proceed to evaluate the integral \mathcal{I}_k given in eq.(6.19). Just like the previous case, here also at first we consider the range $\mu < 0$ and close the contour in the upper half plane and find one first order pole at $\xi = i\nu$ and one second order pole at $\xi = 2\pi ik$. Now, calculating the residues for all poles, taking the limit $\epsilon \rightarrow 0$ and considering both the range $\mu < 0$ and $\mu > 0$, the final result of the integral in eq.(6.19) reads

$$\begin{aligned} \mathcal{I}_k &= \frac{\nu^2 e^{-|\mu|\nu}}{16} \left[\frac{1}{(\nu - 2\pi k)^2} + \frac{1}{(\nu + 2\pi k)^2} \right] + \frac{\nu^2}{64\pi^2} e^{-2\pi k|\mu|} \left[2\pi|\mu| \left\{ \frac{1}{\left(k + \frac{\nu}{2\pi}\right)} - \frac{1}{\left(k - \frac{\nu}{2\pi}\right)} \right\} \right. \\ &\quad \left. + \frac{1}{\left(k + \frac{\nu}{2\pi}\right)^2} - \frac{1}{\left(k - \frac{\nu}{2\pi}\right)^2} \right]. \end{aligned} \quad (6.25)$$

We now employ the Lerch-Hurwitz transcendental function [87],

$$\Phi(z, n, a) = \sum_{k=0}^{\infty} \frac{z^k}{(k+a)^n}. \quad (6.26)$$

Using the above definition of Lerch-Hurwitz transcendental function and the series representation of $\sin^2(\nu/2)$, and taking the summation over k in the eq. (6.25), we finally get

$$\sum_{k=1}^{\infty} \mathcal{I}_k = \frac{e^{-|\mu|\nu}}{16} \left[\frac{(\nu/2)^2}{\sin^2(\nu/2)} - 1 \right] + \frac{\nu^2 e^{-2\pi|\mu|}}{64\pi^2} [2\pi|\mu|\Delta\Phi(\mu, 1, \nu) + \Delta\Phi(\mu, 2, \nu)] \quad (6.27)$$

where $\Delta\Phi(\mu, n, \nu)$ is defined as

$$\Delta\Phi(\mu, n, \nu) = \Phi\left(e^{-2\pi|\mu|}, n, 1 + \frac{\nu}{2\pi}\right) - \Phi\left(e^{-2\pi|\mu|}, n, 1 - \frac{\nu}{2\pi}\right). \quad (6.28)$$

Collecting all these results and substituting them in eq. (6.17), we obtain

$$\mathcal{F}_1(\mu, \nu) = \frac{1}{\hbar c^3} \left[\frac{1}{16} \left(2|\mu|\nu\Theta(-\mu) + \frac{(\nu/2)^2}{\sin^2(\nu/2)} e^{-|\mu|\nu} \right) + \frac{\nu^2 e^{-2\pi|\mu|}}{64\pi^2} [2\pi|\mu|\Delta\Phi(\mu, 1, \nu) + \Delta\Phi(\mu, 2, \nu)] \right]. \quad (6.29)$$

6.1.2 Calculation of $\mathcal{F}_2(\mu, \nu)$

From eq. (6.15), one can find that the poles are situated at

$$\xi = \pm i\nu, \quad \text{and} \quad \xi = \xi^{\pm} \equiv i\epsilon \pm 2 \sinh^{-1}(z). \quad (6.30)$$

All the poles are first order in nature. Now considering the range $\mu < 0$ and closing the contour in the upper half plane, we find that the two first order poles at $\xi = i\nu$ and $\xi = \xi^+$ lie inside the contour. Calculating the residue at $\xi = i\nu$ and taking the limit $\epsilon \rightarrow 0$, we get

$$R_1 = -\frac{e^{\mu\nu}}{2i\nu} \left[\frac{1}{\sin^2(\nu/2) + z^2} \right]. \quad (6.31)$$

Now from eq.(6.15), we can define the function under the integral sign $f(\xi)$ as

$$f(\xi) = \frac{g(\xi)}{h(\xi)} \quad (6.32)$$

where,

$$g(\xi) = \exp(-i\mu\xi) \quad (6.33)$$

$$h(\xi) = (\xi^2 + \nu^2) \left[\sinh^2 \left(\frac{\xi - i\epsilon}{2} \right) - z^2 \right]. \quad (6.34)$$

Calculating the values of $h(\xi)$ and the first derivative of $h(\xi)$ at the point $\xi = \xi^+$, we get

$$h(\xi^+) = 0, \quad h'(\xi^+) \neq 0. \quad (6.35)$$

Since at the point $\xi = \xi^+$, $h(\xi^+) = 0$ but $h'(\xi^+) \neq 0$, therefore residue at the point $\xi = \xi^+$ can be written as

$$R_2 = \frac{g(\xi^+)}{h'(\xi^+)}. \quad (6.36)$$

Calculating this and taking the limit $\epsilon \rightarrow 0$, we find

$$R_2 = \frac{\exp(-2i\mu \sinh^{-1}(z))}{(4 \sinh^{-2}(z) + \nu^2)} \frac{1}{z\sqrt{1+z^2}}. \quad (6.37)$$

This then gives

$$\begin{aligned} \mathcal{F}_2(\mu, \nu) &= \frac{\nu^3}{64\pi\hbar c^3} \times 2\pi i(R_1 + R_2) \\ &= \frac{\nu^3}{64\hbar c^3} \left[-\frac{e^{\mu\nu}}{\nu} \left[\frac{1}{\sin^2(\nu/2) + z^2} \right] + \frac{2i \exp(-2i\mu \sinh^{-1}(z))}{(4 \sinh^{-2}(z) + \nu^2)} \frac{1}{z\sqrt{1+z^2}} \right]. \end{aligned} \quad (6.38)$$

Evaluating eq.(6.15) by considering the range $\mu > 0$, we see that the relevant poles are at $\xi = -i\nu$ and $\xi = \xi^-$. Hence considering both the range $\mu < 0$ and $\mu > 0$, we find

$$\mathcal{F}_2(\mu, \nu) = \frac{\nu^3}{64\hbar c^3} \left[-\frac{e^{-|\mu|\nu}}{\nu} \left[\frac{1}{\sin^2(\nu/2) + z^2} \right] + \frac{2i \exp(2i|\mu| \sinh^{-1}(z))}{(4 \sinh^{-2}(z) + \nu^2)} \frac{1}{z\sqrt{1+z^2}} \right]. \quad (6.39)$$

The real part of $\mathcal{F}_2(\mu, \nu)$ therefore becomes

$$\text{Real } \mathcal{F}_2(\mu, \nu) = -\frac{1}{16\hbar c^3} \frac{(\nu/2)^2 e^{-|\mu|\nu}}{[\sin^2(\nu/2) + z^2]}. \quad (6.40)$$

Substituting eq.(s)(6.29, 6.40) in eq.(6.10), the complete response function turns out to be

$$\begin{aligned} \mathcal{F}(\mu, \nu) = & \frac{1}{\hbar c^3} \left[\frac{1}{16} \left[2|\mu|\nu\Theta(-\mu) + (\nu/2)^2 e^{-|\mu|\nu} \left\{ \frac{1}{\sin^2(\nu/2)} - \frac{1}{[\sin^2(\nu/2) + z^2]} \right\} \right] \right. \\ & \left. + \frac{\nu^2 e^{-2\pi|\mu|}}{64\pi^2} \left[2\pi|\mu|\Delta\Phi(\mu, 1, \nu) + \Delta\Phi(\mu, 2, \nu) \right] \right]. \end{aligned} \quad (6.41)$$

Introducing a new parameter known as the reduced acceleration $a = 1/\mu$, where μ is defined in eq.(6.13), we can recast the response function (in terms of the reduced acceleration and the ratio of the qubit's velocity to that of light in vacuum) as

$$\begin{aligned} \mathcal{F}\left(\frac{1}{a}, 2 \tanh^{-1}(\beta)\right) = & \frac{1}{\hbar c^3} \left[\frac{1}{4|a|} \tanh^{-1}(\beta)\Theta\left(-\frac{1}{a}\right) + \frac{e^{-2\frac{1}{|a|}\tanh^{-1}(\beta)} \tanh^{-2}(\beta)}{16} \left[\frac{1}{\sin^2\{\tanh^{-1}(\beta)\}} \right. \right. \\ & \left. \left. - \frac{1}{[\sin^2\{\tanh^{-1}(\beta)\} + z^2]} \right] + \frac{\tanh^{-2}(\beta)}{16\pi^2} e^{-2\pi\frac{1}{|a|}} \left[2\pi\frac{1}{|a|}\Delta\Phi\left(\frac{1}{a}, 1, 2 \tanh^{-1}(\beta)\right) \right. \right. \\ & \left. \left. + \Delta\Phi\left(\frac{1}{a}, 2, 2 \tanh^{-1}(\beta)\right) \right] \right]. \end{aligned} \quad (6.42)$$

Defining $\Delta\mathcal{F}\left(\frac{1}{a}, 2 \tanh^{-1}(\beta)\right) = -\mathcal{F}\left(\frac{1}{a}, 2 \tanh^{-1}(\beta)\right) + \mathcal{F}\left(-\frac{1}{a}, 2 \tanh^{-1}(\beta)\right)$, we can rewrite eq.(6.1) as

$$\delta p(a, p, \beta) = \lambda_0^2 \left[(1 - 2p) \hbar c^3 \mathcal{F}\left(\frac{1}{a}, 2 \tanh^{-1}(\beta)\right) - p \hbar c^3 \Delta\mathcal{F}\left(\frac{1}{a}, 2 \tanh^{-1}(\beta)\right) \right] \quad (6.43)$$

where from dimensional analysis we fix a dimensionless parameter $\lambda_0 = \sqrt{\lambda^2 c / \hbar^3}$, and $\Delta\mathcal{F}\left(\frac{1}{a}, 2 \tanh^{-1}(\beta)\right)$ is given by where $\Delta\mathcal{F}\left(\frac{1}{a}, 2 \tanh^{-1}(\beta)\right)$ is given by

$$\Delta\mathcal{F}\left(\frac{1}{a}, 2 \tanh^{-1}(\beta)\right) = \frac{1}{\hbar c^3} \left[\frac{1}{4|a|} \tanh^{-1}(\beta) \right]. \quad (6.44)$$

The structure of the response function enables us to demarcate two limiting cases through the condition $\sin^2(\nu/2) \sim z^2$ which defines the intermediate boundary regime. Two other regimes emerge from this definition as we shall see in the subsequent subsections.

6.2 Evaluation of transition probability in the near boundary regime

In the near boundary regime, we have $z^2 \ll \sin^2(\nu/2)$. Hence, carrying out a series expansion of eq.(6.41) for small z , we obtain

$$\begin{aligned} \mathcal{F}(\mu, \nu) = & \frac{1}{\hbar c^3} \left[\frac{1}{16} \left[2|\mu|\nu\Theta(-\mu) + (\nu/2)^2 e^{-|\mu|\nu} \left\{ \frac{z^2}{\sin^4(\nu/2)} \right\} \right] \right. \\ & \left. + \frac{\nu^2 e^{-2\pi|\mu|}}{64\pi^2} \left[2\pi|\mu|\Delta\Phi(\mu, 1, \nu) + \Delta\Phi(\mu, 2, \nu) \right] \right]. \end{aligned} \quad (6.45)$$

Recasting the response function in terms of the reduced acceleration (a) and the ratio of the qubit's velocity to that of light in vacuum, we get

$$\begin{aligned} \mathcal{F}\left(\frac{1}{a}, 2 \tanh^{-1}(\beta)\right) &= \frac{1}{\hbar c^3} \left[\frac{1}{4|a|} \tanh^{-1}(\beta) \Theta\left(-\frac{1}{a}\right) + \frac{e^{-2\frac{1}{|a|} \tanh^{-1}(\beta)} \tanh^{-2}(\beta)}{16} \left[\frac{z^2}{\sin^4\{\tanh^{-1}(\beta)\}} \right] \right. \\ &\quad \left. + \frac{\tanh^{-2}(\beta)}{16\pi^2} e^{-2\pi\frac{1}{|a|}} \left[2\pi \frac{1}{|a|} \Delta\Phi\left(\frac{1}{a}, 1, 2 \tanh^{-1}(\beta)\right) + \Delta\Phi\left(\frac{1}{a}, 2, 2 \tanh^{-1}(\beta)\right) \right] \right] \end{aligned} \quad (6.46)$$

where $\Delta\mathcal{F}\left(\frac{1}{a}, 2 \tanh^{-1}(\beta)\right)$ is given by

$$\Delta\mathcal{F}\left(\frac{1}{a}, 2 \tanh^{-1}(\beta)\right) = \frac{1}{\hbar c^3} \left[\frac{1}{4|a|} \tanh^{-1}(\beta) \right]. \quad (6.47)$$

6.3 Evaluation of transition probability in the far boundary regime

In the far boundary regime, we have $z^2 \gg \sin^2(\nu/2)$. Hence, carrying out a series expansion of eq.(6.41) for large z , we obtain

$$\begin{aligned} \mathcal{F}(\mu, \nu) &= \frac{1}{\hbar c^3} \left[\frac{1}{8} |\mu| \nu \Theta(-\mu) + \frac{e^{-|\mu|\nu}}{16} \left[\frac{(\nu/2)^2}{\sin^2(\nu/2)} - \frac{\nu^2}{4z^2} + \frac{\nu^2}{4z^4} \sin^2(\nu/2) \right] \right. \\ &\quad \left. + \frac{\nu^2}{64\pi^2} e^{-2\pi|\mu|} [2\pi|\mu| \Delta\Phi(\mu, 1, \nu) + \Delta\Phi(\mu, 2, \nu)] \right]. \end{aligned} \quad (6.48)$$

Now recasting the response function in terms of the reduced acceleration a , and the ratio of the qubit's velocity to that of light in vacuum, we get

$$\begin{aligned} \mathcal{F}\left(\frac{1}{a}, 2 \tanh^{-1}(\beta)\right) &= \frac{1}{\hbar c^3} \left[\frac{1}{4|a|} \tanh^{-1}(\beta) \Theta\left(-\frac{1}{a}\right) + \frac{e^{-2\frac{1}{|a|} \tanh^{-1}(\beta)}}{16} \left[\frac{\tanh^{-2}(\beta)}{\sin^2\{\tanh^{-1}(\beta)\}} \right. \right. \\ &\quad \left. \left. - \frac{\tanh^{-2}(\beta)}{z^2} \left(1 - \frac{\sin^2\{\tanh^{-1}(\beta)\}}{z^2} \right) \right] + \frac{\tanh^{-2}(\beta)}{16\pi^2} e^{-2\pi\frac{1}{|a|}} \right. \\ &\quad \left. \times \left[2\pi \frac{1}{|a|} \Delta\Phi\left(\frac{1}{a}, 1, 2 \tanh^{-1}(\beta)\right) + \Delta\Phi\left(\frac{1}{a}, 2, 2 \tanh^{-1}(\beta)\right) \right] \right] \end{aligned} \quad (6.49)$$

where $\Delta\mathcal{F}\left(\frac{1}{a}, 2 \tanh^{-1}(\beta)\right)$ is given by

$$\Delta\mathcal{F}\left(\frac{1}{a}, 2 \tanh^{-1}(\beta)\right) = \frac{1}{\hbar c^3} \left[\frac{1}{4|a|} \tanh^{-1}(\beta) \right]. \quad (6.50)$$

7 Analysis of thermodynamical steps

In this section, we will analyse each thermodynamical step of the UQOE in the presence of a reflecting boundary and calculate the amount of heat exchanged between the qubit and the quantum vacuum and the amount of work done by the qubit.

7.1 Adiabatic expansion

In this step, the form of the initial state of the qubit $\rho_0 = p|e\rangle\langle e| + (1-p)|g\rangle\langle g|$ remains fixed and the energy gap between the energy levels changes from \mathcal{E}_1 to a higher value \mathcal{E}_2 over a time \mathcal{T} . The time-dependent Hamiltonian of the qubit is given by

$$\mathcal{H}(t) = \mathcal{E}(t)|e\rangle\langle e|. \quad (7.1)$$

Using the definition of the average heat transfer eq.(2.2), we find that this step is purely adiabatic, i.e.,

$$\langle Q_1 \rangle = \int_0^{\mathcal{T}} dt \text{Tr} \left[\frac{\partial \rho_0}{\partial t} \mathcal{H}(t) \right] = 0. \quad (7.2)$$

In a similar way, using the expression of average work done eq.(2.3), we find that there is a positive work done on the system, given by

$$\begin{aligned} \langle W_1 \rangle &= \int_0^{\mathcal{T}} dt \text{Tr} \left[\rho_0 \frac{\partial \mathcal{H}(t)}{\partial t} \right] \\ &= \int_0^{\mathcal{T}} d\mathcal{E} \text{Tr} [\rho_0 |e\rangle\langle e|] \\ &= p(\mathcal{E}_2 - \mathcal{E}_1). \end{aligned} \quad (7.3)$$

7.2 Contact with the hot vacuum

In this step, the Hamiltonian of the system is fixed at a constant value $\mathcal{H} = \mathcal{E}_2|e\rangle\langle e|$. The qubit accelerates from v to $-v$ over the interval \mathcal{T}_2 and interacts with the background quantum field. During this time the qubit's state evolves through the interaction with the background quantum field as shown in section 4 and takes the form

$$\rho_{\mathcal{T}_2} = \rho_0 + \delta p_H \sigma_3 \quad (7.4)$$

where $\sigma_3 = |e\rangle\langle e| - |g\rangle\langle g|$ and $\delta p_H = \delta p_{\mathcal{T}_2}$. No work is done in this step due to the constant value of the qubit Hamiltonian and hence, we get

$$\langle W_2 \rangle = \int_0^{\mathcal{T}_2} dt \text{Tr} \left[\rho(t) \frac{\partial \mathcal{H}(t)}{\partial t} \right] = 0. \quad (7.5)$$

On the other hand, the system absorbs heat from the vacuum, given by

$$\begin{aligned} \langle Q_2 \rangle &= \int_0^{\mathcal{T}_2} dt \text{Tr} \left[\frac{\partial \rho(t)}{\partial t} \mathcal{H} \right] = \int_0^{\mathcal{T}_2} dt \text{Tr} \left[\frac{\partial \delta p(t)}{\partial t} \mathcal{E}_2 \sigma_3 |e\rangle\langle e| \right] \\ &= \mathcal{E}_2 \int_0^{\mathcal{T}_2} \text{Tr} [\partial \delta p(t) \sigma_3 |e\rangle\langle e|] = \mathcal{E}_2 \text{Tr} [\delta p_H \sigma_3 |e\rangle\langle e|] \\ &= \mathcal{E}_2 \delta p_H. \end{aligned} \quad (7.6)$$

7.3 Adiabatic contraction

In this step, the qubit travels at velocity $-v$ and the state ρ is held fixed at $\rho = \rho_0 + \delta p_H \sigma_3$ as the energy gap is reduced from \mathcal{E}_2 to \mathcal{E}_1 . Just like the adiabatic expansion, no heat is exchanged, and we have

$$\langle Q_3 \rangle = 0 \quad (7.7)$$

and the value of work done is

$$\langle W_3 \rangle = -(\mathcal{E}_2 - \mathcal{E}_1)(p + \delta p_H). \quad (7.8)$$

7.4 Contact with the cold vacuum

In the final step, the Hamiltonian of the system is again fixed at another constant value $\mathcal{H} = \mathcal{E}_1 |e\rangle\langle e|$. The qubit accelerates from $-v$ to $+v$ over the interval \mathcal{T}_1 and interacts with the background quantum field. Therefore, just like the hot vacuum case the state of the qubit evolves and takes the form

$$\rho_{\mathcal{T}_1} = \rho_1 + \delta p_C \sigma_3 \quad (7.9)$$

where $\rho_1 = p'|e\rangle\langle e| + (1-p')|g\rangle\langle g|$, $\delta p_C = \delta p_{\mathcal{T}_1}$ and $p' = p + \delta p_H$. Here also we get no work done

$$\langle W_4 \rangle = 0 \quad (7.10)$$

and the average heat transfer is

$$\langle Q_4 \rangle = \mathcal{E}_1 \delta p_C. \quad (7.11)$$

7.5 Completing the cycle

From the above analysis we have already calculated and got the amount of heat exchanged and work done in each step of the thermodynamical cycle. Now, for returning the qubit to its initial state and completing the cycle, we have to impose the condition $\delta p_H + \delta p_C = 0$. The total amount of heat transfer and the net work done by the cycle is then

$$\langle W_{\text{tot}} \rangle = \langle W_1 \rangle + \langle W_3 \rangle = -(\mathcal{E}_2 - \mathcal{E}_1) \delta p_H \quad (7.12)$$

$$\langle Q_{\text{tot}} \rangle = \langle Q_2 \rangle + \langle Q_4 \rangle = (\mathcal{E}_2 - \mathcal{E}_1) \delta p_H \quad (7.13)$$

which obeys the conservation of energy as

$$\langle W_{\text{tot}} \rangle + \langle Q_{\text{tot}} \rangle = 0. \quad (7.14)$$

In case of the quantum thermal engine (QOE) discussed in section 2, after exchanging the heat with the hot and cold reservoirs, the qubit state satisfies

$$p + \delta p_H = \text{Tr}[|e\rangle\langle e|\rho] = 1/(1 + \exp(\mathcal{E}_2/k_B T_H)) \quad (7.15)$$

$$p = \text{Tr}[|e\rangle\langle e|\rho_{\text{final}}] = 1/(1 + \exp(\mathcal{E}_1/k_B T_C)). \quad (7.16)$$

Therefore, the transition probability of the QOE can be written as

$$\delta p = \frac{1}{(1 + \exp(\mathcal{E}_2/k_B T_H))} - \frac{1}{(1 + \exp(\mathcal{E}_1/k_B T_C))}. \quad (7.17)$$

Hence, for getting positive work, eq.(7.17) suggests that $\delta p > 1$ which in turn leads to the condition

$$T_H/\mathcal{E}_2 > T_C/\mathcal{E}_1 \quad (7.18)$$

which is much stronger than its classical analogue $T_H > T_C$.

8 Results

In this section we analyse our findings for three different cases, namely, near boundary regime, intermediate boundary regime and far boundary regime of UQOE in the presence of a single reflecting boundary.

8.1 Demarcation of regimes with respect to the parameters

We first estimate the value of z which depends on the acceleration of the qubit (α) and z_0 , for different regimes. Studies in the context of trapped ultracold atoms [88] and superconducting circuits [80] show that these quantum systems are effective to practically realize atom-field interactions due to accelerating qubits. In such systems taking the ultrafast variation of the qubit-field coupling, it has been possible to achieve large acceleration up to $7 \times 10^{17} m/s^2$ [52]. In our analysis we choose the parameters mimicking the values for the above systems to a certain extent. Thus, during the first qubit-field interaction for a particular cycle, we take the value $\alpha = 6 \times 10^{17} m/s^2$, and note that in the intermediate boundary regime $\sin^2(\frac{\alpha T}{2c}) \sim z^2$. Hence setting $\sin^2(\frac{\alpha T}{2c}) = 1 = z^2$ fixes $\mathcal{T} = 16 \times 10^{-9} s$ and $z_0 = 15 cm$. Similarly, for the second qubit-field interaction in that same cycle we choose $\alpha = 3 \times 10^{17} m/s^2$. This fixes $\mathcal{T} = 31 \times 10^{-9} s$ and $z_0 = 30 cm$ in the intermediate boundary regime. With these choice of parameters, we now have three distinct regimes shown in Table 1.

Regime	z	z_{0H} (cm)	z_{0C} (cm)
Near	less than 1	less than 15	less than 30
Intermediate	equal to 1	equal to 15	equal to 30
Far	greater than 1	greater than 15	greater than 30

Table 1: Three different regimes in a particular thermodynamical cycle with $\alpha_H = 6 \times 10^{17} m/s^2$ and $\alpha_C = 3 \times 10^{17} m/s^2$.

8.2 Transition probability

We have already seen from our calculations, the transition probability δp between two energy levels of the qubit depends on various parameters. Here we plot the behaviour of the transition probability between two energy levels of the qubit with respect to reduced acceleration a in three different regimes, namely, intermediate, near and far boundary regime, respectively, for various values of p , β and z in Figures 5, 6 and 7 respectively. Following the estimation given in Table 1, we consider $z = 0.5$ for the near boundary regime, $z = 1$ for intermediate boundary regime and $z = 3$ for far boundary regime. For each regime we consider four qubit velocities $\beta = 0.5, 0.6, 0.7, 0.8$.

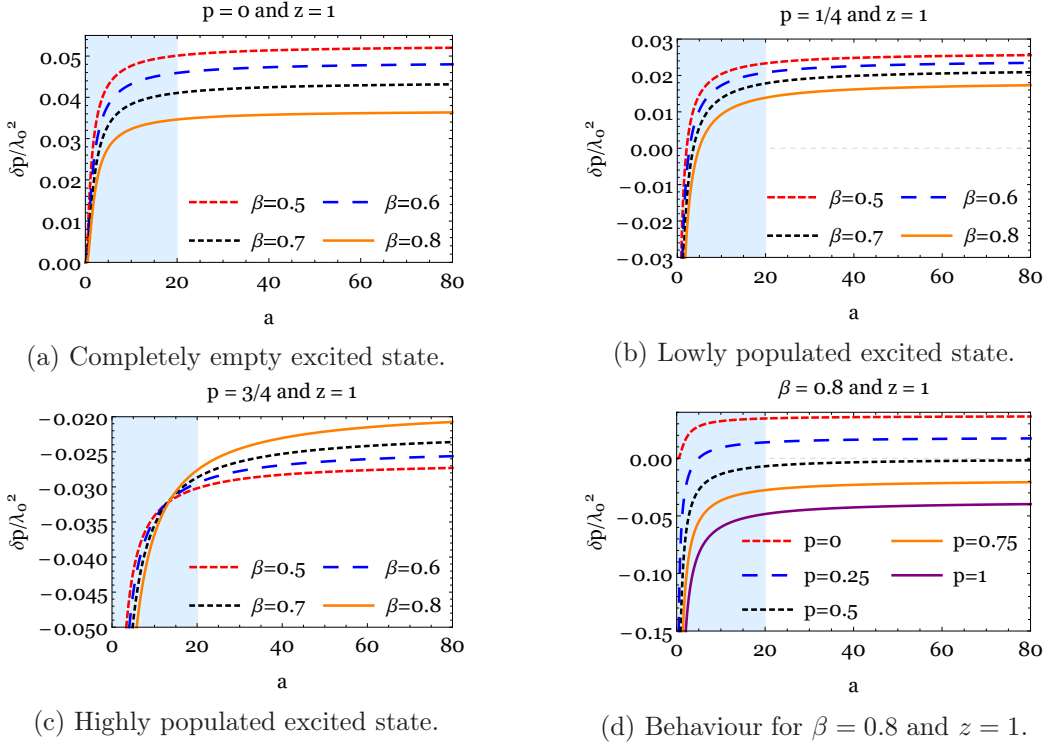


Figure 5: Behaviour of the transition probability with respect to reduced acceleration a in the intermediate boundary regime for various values of p and β .

From Figure 5, it is observed that in the intermediate boundary regime, the transition probability corresponding to each qubit velocity β ubiquitously increases with the increment of reduced acceleration, and from Unruh effect it is directly associated with the increment of temperature. The shaded blue region shows the region where the perturbative scheme breaks down for small a , and δp diverges for $p \neq 0$.

The transition probability eq.(6.43), for the case where the probability of a qubit being in the excited state is zero ($p = 0$), is plotted in Figure 5a. Here we observe that the transition probability δp is always positive for all four chosen qubit velocities. Comparing with the UQOE without any reflecting boundary [64, 65], we observe that for a particular value of reduced acceleration a , the transition probability decreases with the increase of

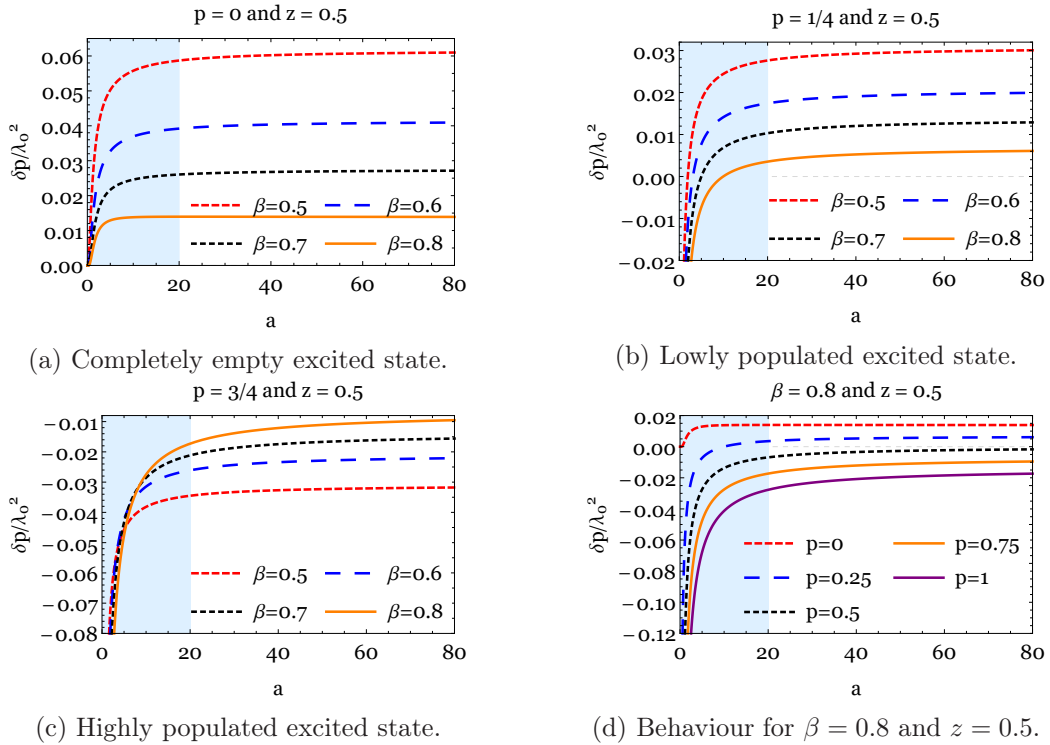


Figure 6: Behaviour of the transition probability with respect to reduced acceleration a in the near boundary regime for various values of p and β .

parameter β .

In Figure 5b, the transition probability for the case where the qubit has a lowly populated excited state ($p = 1/4$) is plotted. As the excited state is lowly populated, the value of δp is lesser here. Divergence occurs in the region where reduced acceleration is very low. In Figure 5c, an initially highly populated qubit state ($p = 3/4$) is plotted. In this case δp is negative, which indicates that due to a less populated ground state after the interaction of the quantum field, a de-excitation process occurs. In Figure 5d, different initial excitation probabilities for a fixed value of β and z are plotted. Here we get positive transition probability δp for the value $p = 0$ for all values of a . For $0 < p < 1/2$, δp is initially negative for lower values of a and becomes positive for higher values of a . However we get negative δp for the value $1 > p > 1/2$ for all values of a . For the critical value $p = 1/2$, δp is initially negative and approaches to zero as the value of a increases.

We now display our results for the near boundary regime. From the Figures, it is also observed that for a particular value of β , δp continuously increases with the increment of reduced acceleration. For small values of reduced acceleration a , the perturbative scheme breaks down and δp diverges for all $p \neq 0$ cases. From Figure 6a, it is seen that for the case where the probability of a qubit being in the excited state is zero ($p = 0$), δp remains positive but due to the effect of the reflecting boundary, it is observed that as the distance between the reflecting boundary and the qubit decreases compared to the intermediate boundary regime for a particular reduced acceleration, the transition probability for higher

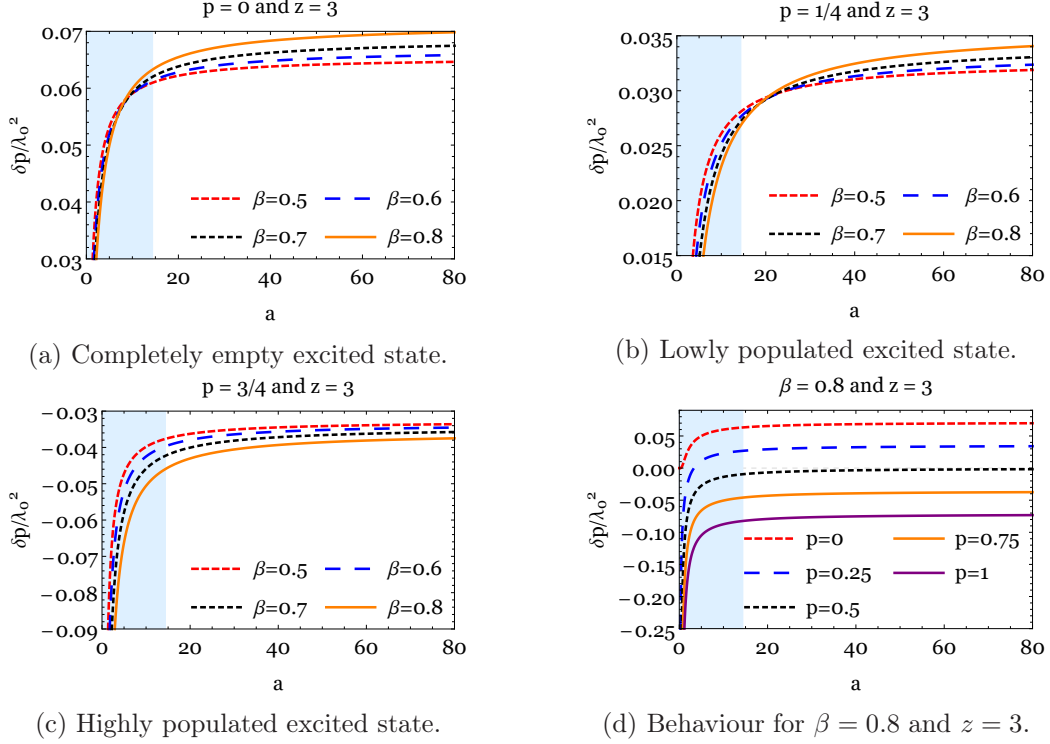


Figure 7: Behaviour of the transition probability with respect to reduced acceleration a in the far boundary regime for various values of p and β .

qubit velocity decreases rapidly compared to the intermediate boundary regime. From Figure 6b, we again observe similar behaviour (as the intermediate boundary regime) of the transition probability for the lowly populated excited state of the qubit ($p = 1/4$). In Figure 6c, transition probability corresponding to an initially highly populated qubit state, $p = 3/4$ is plotted. In this case δp is also negative in nature. In Figure 6d, different initial excitation probabilities for a fixed value of β are plotted. Here we gain observe similar behaviour with Figure 5d.

Next, considering the far boundary regime, from Figure 7, it is observed that the nature of the Figure 7a, 7b and 7c are qualitatively similar to the Figure 5a, 5b and 5c, except that for a particular value of reduced acceleration, the transition probability increases with increase in the qubit velocity, which happens in the case of UQOE without any reflecting boundary [64, 65]. Here we once again observe that in the far boundary limit δp remains always positive for the case where the probability of a qubit being in the excited state is zero ($p = 0$). Here too, Figure 7d shows the variation of δp with different initial excitation probabilities for a fixed value of β . As expected, the far boundary regime yields results that approach the case of UQOE without any reflecting boundary [64, 65].

The impact of the reflecting boundary is further clearly revealed through a comparison between the behaviour of the transition probability with respect to reduced acceleration a in the intermediate, near and far boundary regimes, as plotted in Figures (5a, 6a, 7a), respectively. It can be seen that when the reflecting boundary is close to the qubit, for a

fixed value of reduced acceleration the transition probability decreases with the increase of parameter β . In the intermediate regime, it is observed that for a fixed value of reduced acceleration, the transition probability still decreases with the increase of parameter β , but the transition probability corresponding to the higher qubit velocity is greater than the corresponding value in the near boundary limit. Interestingly, shifting the reflecting boundary further, we find that in the far boundary limit, for a fixed value of reduced acceleration, the transition probability increases with the increase of parameter β . However, for fixed values of p , β and a , the transition probability increases when the distance between the reflecting boundary and the qubit is increased. This occurs because, as the distance between the boundary and the qubit is increased, more number of field modes take part in the interaction between the scalar field and the qubit, which in turn increases the transition probability. Hence, the behaviour of transition probability shows the effect of the reflecting boundary clearly.

8.3 Work output in the presence of a reflecting boundary

In this subsection we calculate the work output of the UQOE in the presence of a reflecting boundary. We have seen earlier that presence of the reflecting boundary does not affect qubit's thermodynamical steps. To calculate the work output of the UQOE, at first we have to ensure that the thermodynamical cycle is closed. In order to achieve the cyclicity of the UQOE in presence of the boundary, we employ the constraint condition,

$$\delta p_H(a_H, p, \beta) + \delta p_C(a_C, p, \beta) = 0. \quad (8.1)$$

Substituting eq.(6.43) in the above constraint condition eq.(8.1), we get

$$(1 - 2p) \left[\mathcal{F} \left(\frac{1}{a_H}, 2 \tanh^{-1}(\beta) \right) + \mathcal{F} \left(\frac{1}{a_C}, 2 \tanh^{-1}(\beta) \right) \right] = p \left[\Delta \mathcal{F} \left(\frac{1}{a_H}, 2 \tanh^{-1}(\beta) \right) + \Delta \mathcal{F} \left(\frac{1}{a_C}, 2 \tanh^{-1}(\beta) \right) \right]. \quad (8.2)$$

Therefore

$$\frac{p}{1 - 2p} = \frac{\mathcal{F} \left(\frac{1}{a_H}, 2 \tanh^{-1}(\beta) \right) + \mathcal{F} \left(\frac{1}{a_C}, 2 \tanh^{-1}(\beta) \right)}{\Delta \mathcal{F} \left(\frac{1}{a_H}, 2 \tanh^{-1}(\beta) \right) + \Delta \mathcal{F} \left(\frac{1}{a_C}, 2 \tanh^{-1}(\beta) \right)}. \quad (8.3)$$

Defining \mathcal{P} as

$$\mathcal{P} \equiv \frac{\mathcal{F} \left(\frac{1}{a_H}, 2 \tanh^{-1}(\beta) \right) + \mathcal{F} \left(\frac{1}{a_C}, 2 \tanh^{-1}(\beta) \right)}{\Delta \mathcal{F} \left(\frac{1}{a_H}, 2 \tanh^{-1}(\beta) \right) + \Delta \mathcal{F} \left(\frac{1}{a_C}, 2 \tanh^{-1}(\beta) \right)}. \quad (8.4)$$

the initial population of the excited state of the qubit turns out to be

$$p = \frac{\mathcal{P}}{1 + 2\mathcal{P}}. \quad (8.5)$$

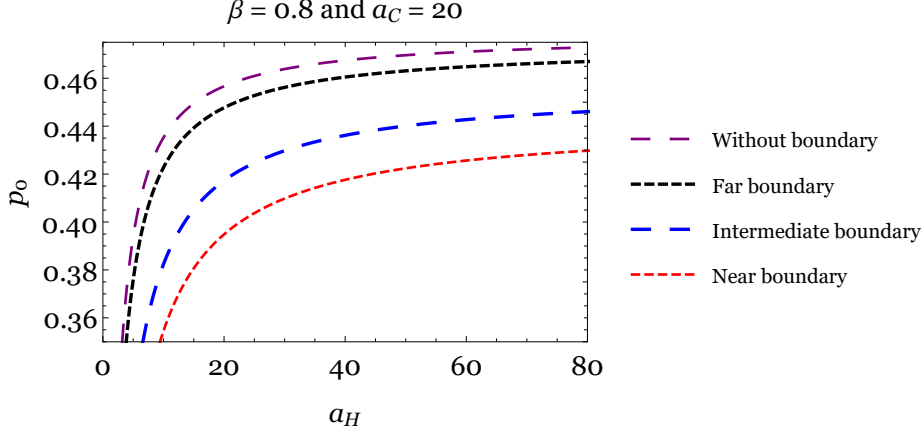


Figure 8: Behaviour of the critical probability p_0 with respect to a_H for fixed values of β and a_C .

We define this initial excited state probability p as the critical probability p_0 , to ensure that the vacuum acts as a hot and cold reservoir, at the same value of p_0 for the qubit with reduced acceleration a_H and a_C , respectively. The closure of the cycle is ensured and the qubit returns to its initial state for this particular value. From the thermodynamical analysis, we have already seen that during the first interaction with the vacuum, the qubit absorbs heat from the vacuum fluctuation and $\delta p(a_H, p, \beta) > 0$. From figure(s)(5, 6, 7), it is seen that δp is positive only when initial excited state probability $p = 0$.

The behaviour of the critical excitation probability p_0 with respect to a_H is displayed in Figure 8 for fixed values of $\beta = 0.8$ and $a_C = 20$. From the figure it is observed that the reflecting boundary reduces the critical probability of the qubit p_0 . For a fixed value of a_H , we find that when the reflecting boundary is at a near distance, the critical probability of the excited state of the qubit having velocity $\beta = 0.8$ is minimum and it gradually increases with increase in the boundary distance. In the presence of the boundary, the critical probability p_0 is also found to be bounded from both ends, i.e., $0 \leq p_0 < 1/2$, which is consistent with the Figure(s)(5, 6, 7). Now, using the value of p_0 , we can recast the transition probability of the qubit $\delta \bar{p}_H$ as

$$\delta \bar{p}_H = \delta p(a_H, p_0, \beta), \quad (8.6)$$

which automatically ensures that the cyclic condition is satisfied.

Next, considering eq.(7.12) we can write down the amount of total work done by the UQOE in presence of the reflecting boundary as

$$W \equiv \langle W_{ext} \rangle = (\mathcal{E}_2 - \mathcal{E}_1) \delta \bar{p}_H. \quad (8.7)$$

In Figure 9, we plot the amount of output work as a function of a_H for fixed values of $\beta = 0.8$ and $a_C = 20$ by taking $\mathcal{E}_2 - \mathcal{E}_1 = 1$. From the figure it is observed that in our model of relativistic quantum thermal heat engine, the work output depends on the position

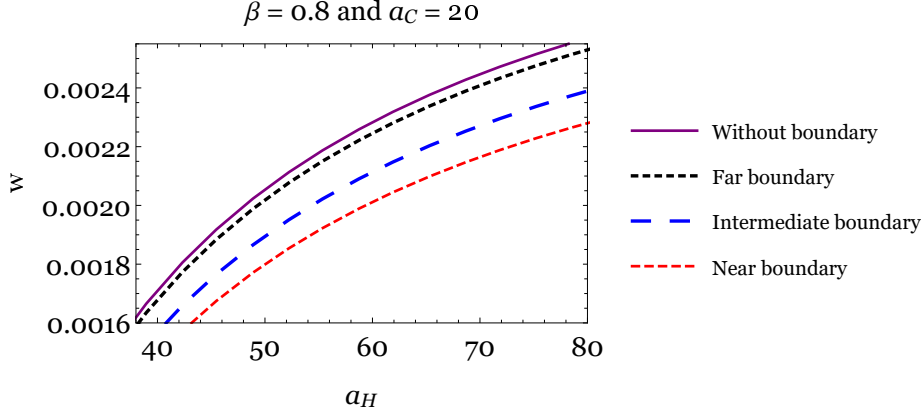


Figure 9: Behaviour of the work output with respect to a_H for fixed values of β and a_C .

of the reflecting boundary. Comparing with the work output of the UQOE [64], we observe that in the near mirror limit the work output is minimum, and it gradually increases with increase in the distance between the boundary and the qubit. This is consistent with the fact that the critical probability p_0 is a monotonic function with respect to the location of the boundary (see Figure 8). We also observe that when $a_H > a_C$, the cycle behaves as a thermal machine and positive work is done. In order to act as a thermal machine, the system absorbs heat from the hot quantum vacuum $\delta\bar{p}_H > 0$, which in turn implies the condition,

$$\alpha_H/\mathcal{E}_2 > \alpha_C/\mathcal{E}_1. \quad (8.8)$$

Therefore, we also find a similar condition for UQOE in the presence of a reflecting boundary, which is the same as eq.(7.18), and is stronger compared to its classical counterpart.

The net work done by the engine and total amount of heat transfer between the qubit and the quantum vacuum in the presence of the reflecting boundary is given by eq(s).(7.12, 7.13). We have found that the values of these quantities satisfy the energy conservation principle. From the expressions eq(s).(7.12, 7.13), we can calculate the efficiency of the heat engine. Since we have employed external stimulation to change the energy gap of the qubit levels during the adiabatic expansion and contraction discussed in section 7, therefore, the amount of work done by the qubit is $\langle W_{\text{ext}} \rangle = -\langle W \rangle$. Hence, the efficiency is given by

$$\eta = \frac{\langle W_{\text{ext}} \rangle}{Q_2} = 1 - \frac{\mathcal{E}_1}{\mathcal{E}_2} \quad (8.9)$$

It may be noted that as Q_2 is also proportional to $\delta\bar{p}_H$, therefore, the amount of absorbed heat is also reduced in the presence of a reflecting boundary. Hence, from eq.(8.9) it is observed that the efficiency in our model is independent of any boundary effect. It only depends on the energy gap ratio between the two levels of the qubit and takes a form identical to the UQOE without any boundary [64–66].

9 Conclusions

In this paper, we have proposed a model for the relativistic quantum analogue of the classical Otto heat engine. In our model, a uniformly accelerated qubit (Unruh-DeWitt detector) acts as the working substance, and is coupled to a massless quantum scalar field in the presence of a perfectly reflecting boundary which obeys the Dirichlet boundary condition. The reflecting boundary is the new ingredient that we introduce in our work, which has important physical consequences. Using the notion of the Unruh effect, the quantum vacuum behaves as a thermal bath, and we have uncovered certain interesting features associated with the process of work extraction from the quantum vacuum fluctuations of a quantum scalar field in the presence of a reflecting boundary.

It has been observed earlier that the correlation function between scalar fields, commonly known as the Wightman function, gets significantly modified by the presence of a reflecting boundary [73]. Since the response function of the qubit depends on this correlation function [74–77], an extra contribution due to the presence of the reflecting boundary appears [64, 65]. From the structure of this correlation function, we find that three different cases emerge, i.e., the near boundary regime, the intermediate boundary regime, and the far boundary regime. We show that the near boundary case is the one where the role of the reflecting boundary is most prominently felt, and the far boundary limit corresponds to the case in which one can smoothly go to the case where the boundary is absent. Choosing experimentally realizable values of the qubit acceleration and the distance between the qubit and the reflecting boundary, we estimate a parameter which determines the applicability of each approximation limit.

Our analysis leads to several interesting results. We find that when the reflecting boundary is close to the qubit, for a fixed value of qubit acceleration the transition probability decreases with the increase of the qubit velocity. In the intermediate limit, it is observed that the transition probability corresponding to a higher qubit velocity is greater than the corresponding value in the near boundary limit. Shifting the boundary further, we find that in the far boundary limit the transition probability starts increasing with increase in the qubit velocity for a particular value of qubit acceleration. The effect of the reflecting boundary is clearly manifested through the behaviour of the atomic transition probability.

We further observe that the reflecting boundary reduces the critical probability of the qubit compared to the Unruh quantum Otto engines (UQOE) [64] without a boundary. For a fixed value of a_H , we find that when the reflecting boundary is at a near distance, the critical probability of the excited state of the qubit is minimum and it gradually increases with increase in the distance between the reflecting boundary and the qubit. This reveals that the critical probability is a monotonically increasing function of the distance between the reflecting boundary and the qubit. Next, comparing the work output of this new model with the usual UQOE [64], we find that the work extraction gets inhibited due to the presence of the reflecting boundary. It is observed that the output work of this quantum relativistic heat engine depends on the position of the reflecting boundary, and maximum work output is obtained when the distance between the qubit and the reflecting boundary is maximum. Furthermore, we also observe that the work output is also a monotonically

increasing function of the distance between the reflecting boundary and the qubit. This is compatible with the result obtained for the critical excitation probability. However, for the entire cycle, it is observed that the efficiency of our engine is identical to that of the usual UQOE.

Our approach opens up several new directions for further studies. First, our model of relativistic quantum thermal machine can be probed further without the linearized approximation by considering higher order of interactions. Secondly, it would be interesting to explore whether the boundary effects on relativistic heat engines may be reversed using fermionic quantum fields. Finally, this work can also be extended to the domain of an experimental superconducting cavity setup [19] in order to verify the boundary effects on the efficiency and work output of the model proposed here.

Acknowledgement

AM and ASM acknowledges support from project no. DST/ICPS/QuEST/2019/Q79 of the Department of Science and Technology (DST), Government of India. The authors would also like to thank the referees for very useful comments and suggestions.

References

- [1] J. Gemmer, M. Michel and G. Mahler, *Quantum thermodynamics: Emergence of thermodynamic behavior within composite quantum systems*, vol. 784, Springer (2009), [10.1007/978-3-540-70510-9](https://doi.org/10.1007/978-3-540-70510-9).
- [2] R. Kosloff, *Quantum thermodynamics: A dynamical viewpoint*, *Entropy* **15** (2013) 2100.
- [3] R. Alicki and R. Kosloff, *Introduction to quantum thermodynamics: History and prospects*, in *Thermodynamics in the Quantum Regime*, pp. 1–33, Springer (2018), DOI.
- [4] S. Deffner and S. Campbell, *Quantum Thermodynamics: An introduction to the thermodynamics of quantum information*, Morgan & Claypool Publishers (2019), [10.1088/2053-2571/ab21c6](https://doi.org/10.1088/2053-2571/ab21c6).
- [5] V. Vedral and E. Kashefi, *Uniqueness of the entanglement measure for bipartite pure states and thermodynamics*, *Physical review letters* **89** (2002) 037903.
- [6] F.G. Brandao, M. Horodecki, J. Oppenheim, J.M. Renes and R.W. Spekkens, *Resource theory of quantum states out of thermal equilibrium*, *Physical review letters* **111** (2013) 250404.
- [7] Y. Rezek and R. Kosloff, *Irreversible performance of a quantum harmonic heat engine*, *New Journal of Physics* **8** (2006) 83.
- [8] H. Wang, S. Liu and J. He, *Performance analysis and parametric optimum criteria of a quantum otto heat engine with heat transfer effects*, *Applied thermal engineering* **29** (2009) 706.
- [9] S. Abe and S. Okuyama, *Similarity between quantum mechanics and thermodynamics: Entropy, temperature, and carnot cycle*, *Physical Review E* **83** (2011) 021121.
- [10] G. Thomas and R.S. Johal, *Coupled quantum otto cycle*, *Physical Review E* **83** (2011) 031135.

- [11] R. Kosloff and Y. Rezek, *The quantum harmonic otto cycle*, [*Entropy* **19** \(2017\) 136](#).
- [12] G. Agarwal and S. Chaturvedi, *Quantum dynamical framework for brownian heat engines*, [*Physical Review E* **88** \(2013\) 012130](#).
- [13] J. Roßnagel, O. Abah, F. Schmidt-Kaler, K. Singer and E. Lutz, *Nanoscale heat engine beyond the carnot limit*, [*Phys. Rev. Lett.* **112** \(2014\) 030602](#).
- [14] M. Azimi, L. Chotorlishvili, S.K. Mishra, T. Vekua, W. Hübner and J. Berakdar, *Quantum otto heat engine based on a multiferroic chain working substance*, [*New Journal of Physics* **16** \(2014\) 063018](#).
- [15] X. Zhang, X. Huang and X. Yi, *Quantum otto heat engine with a non-markovian reservoir*, [*Journal of Physics A: Mathematical and Theoretical* **47** \(2014\) 455002](#).
- [16] E. Ivanchenko, *Quantum otto cycle efficiency on coupled qudits*, [*Physical Review E* **92** \(2015\) 032124](#).
- [17] R.J. de Assis, T.M. de Mendonça, C.J. Villas-Boas, A.M. de Souza, R.S. Sarthour, I.S. Oliveira et al., *Efficiency of a quantum otto heat engine operating under a reservoir at effective negative temperatures*, [*Physical Review Letters* **122** \(2019\) 240602](#).
- [18] P.A. Camati, J.F. Santos and R.M. Serra, *Coherence effects in the performance of the quantum otto heat engine*, [*Physical Review A* **99** \(2019\) 062103](#).
- [19] N.F. Del Grosso, F.C. Lombardo, F.D. Mazzitelli and P.I. Villar, *Quantum otto cycle in a superconducting cavity in the nonadiabatic regime*, [*Physical Review A* **105** \(2022\) 022202](#).
- [20] T.D. Kieu, *The second law, maxwell's demon, and work derivable from quantum heat engines*, [*Physical review letters* **93** \(2004\) 140403](#).
- [21] T.D. Kieu, *Quantum heat engines, the second law and maxwell's daemon*, [*The European Physical Journal D* **39** \(2006\) 115](#).
- [22] H.-T. Quan, Y.-x. Liu, C.-P. Sun and F. Nori, *Quantum thermodynamic cycles and quantum heat engines*, [*Physical Review E* **76** \(2007\) 031105](#).
- [23] H.T. Quan, *Quantum thermodynamic cycles and quantum heat engines. ii.*, [*Physical Review E* **79** \(2009\) 041129](#).
- [24] K. Maruyama, F. Nori and V. Vedral, *Colloquium: The physics of maxwell's demon and information*, [*Reviews of Modern Physics* **81** \(2009\) 1](#).
- [25] J.D. Bekenstein, *Black holes and the second law*, in *JACOB BEKENSTEIN: The Conservative Revolutionary*, pp. 303–306, World Scientific (2020), [DOI](#).
- [26] J.M. Bardeen, B. Carter and S.W. Hawking, *The four laws of black hole mechanics*, [*Communications in mathematical physics* **31** \(1973\) 161](#).
- [27] S.W. Hawking, *Particle creation by black holes*, in *Euclidean quantum gravity*, pp. 167–188, World Scientific (1975), [DOI](#).
- [28] S.W. Hawking, *Black holes and thermodynamics*, [*Physical Review D* **13** \(1976\) 191](#).
- [29] W.G. Unruh, *Notes on black-hole evaporation*, [*Physical Review D* **14** \(1976\) 870](#).
- [30] N. Papadatos and C. Anastopoulos, *Relativistic quantum thermodynamics of moving systems*, [*Physical Review D* **102** \(2020\) 085005](#).
- [31] P. Chattopadhyay and G. Paul, *Relativistic quantum heat engine from uncertainty relation standpoint*, [*Scientific reports* **9** \(2019\) 1](#).

- [32] N. Papadatos, *The quantum otto heat engine with a relativistically moving thermal bath*, *International Journal of Theoretical Physics* **60** (2021) 4210.
- [33] N.M. Myers, O. Abah and S. Deffner, *Quantum otto engines at relativistic energies*, *New Journal of Physics* **23** (2021) 105001.
- [34] S. Hawking and W. Israel, *General Relativity: an Einstein Centenary Survey* (2010).
- [35] G.T. Moore, *Quantum theory of the electromagnetic field in a variable-length one-dimensional cavity*, *Journal of Mathematical Physics* **11** (1970) 2679.
- [36] S.A. Fulling and P.C. Davies, *Radiation from a moving mirror in two dimensional space-time: conformal anomaly*, *Proceedings of the Royal Society of London. A. Mathematical and Physical Sciences* **348** (1976) 393.
- [37] P.C. Davies and S.A. Fulling, *Radiation from moving mirrors and from black holes*, *Proceedings of the Royal Society of London. A. Mathematical and Physical Sciences* **356** (1977) 237.
- [38] B.A. Juárez-Aubry and J. Louko, *Quantum fields during black hole formation: how good an approximation is the unruh state?*, *Journal of High Energy Physics* **2018** (2018) .
- [39] W. Cong, C. Qian, M.R. Good and R.B. Mann, *Effects of horizons on entanglement harvesting*, *Journal of High Energy Physics* **2020** (2020) .
- [40] J.H. Wilson, F. Sorge and S.A. Fulling, *Tidal and nonequilibrium casimir effects in free fall*, *Physical Review D* **101** (2020) 065007.
- [41] M.R. Good, K. Yelshibekov and Y.C. Ong, *On horizonless temperature with an accelerating mirror*, *Journal of High Energy Physics* **2017** (2017) .
- [42] M.R. Good, Y.C. Ong, A. Myrzakul and K. Yelshibekov, *Information preservation for null shell collapse: A moving mirror model*, *General Relativity and Gravitation* **51** (2019) .
- [43] D. Fernández-Silvestre, J. Foo and M.R. Good, *On the duality of schwarzschild-de sitter spacetime and moving mirror*, *Classical and Quantum Gravity* (2022) .
- [44] A. Myrzakul, C. Xiong and M.R. Good, *Cghs black hole analog moving mirror and its relativistic quantum information as radiation reaction*, *Entropy* **23** (2021) 1664.
- [45] E. Vetsch, D. Reitz, G. Sagué, R. Schmidt, S.T. Dawkins and A. Rauschenbeutel, *Optical interface created by laser-cooled atoms trapped in the evanescent field surrounding an optical nanofiber*, *Phys. Rev. Lett.* **104** (2010) 203603.
- [46] A. Goban, K.S. Choi, D.J. Alton, D. Ding, C. Lacroûte, M. Pototschnig et al., *Demonstration of a state-insensitive, compensated nanofiber trap*, *Phys. Rev. Lett.* **109** (2012) 033603.
- [47] N.V. Corzo, J. Raskop, A. Chandra, A.S. Sheremet, B. Gouraud and J. Laurat, *Waveguide-coupled single collective excitation of atomic arrays*, *Nature* **566** (2019) 359.
- [48] J.D. Thompson, T.G. Tiecke, N.P. de Leon, J. Feist, A.V. Akimov, M. Gullans et al., *Coupling a single trapped atom to a nanoscale optical cavity*, *Science* **340** (2013) 1202.
- [49] P. Solano, J.A. Grover, J.E. Hoffman, S. Ravets, F.K. Fatemi, L.A. Orozco et al., *Chapter seven - optical nanofibers: A new platform for quantum optics*, vol. 66 of *Advances In Atomic, Molecular, and Optical Physics*, pp. 439–505, Academic Press (2017), DOI.
- [50] D.E. Chang, J.S. Douglas, A. González-Tudela, C.-L. Hung and H.J. Kimble, *Colloquium: Quantum matter built from nanoscopic lattices of atoms and photons*, *Rev. Mod. Phys.* **90** (2018) 031002.

- [51] N. Friis, A.R. Lee, K. Truong, C. Sabín, E. Solano, G. Johansson et al., *Relativistic quantum teleportation with superconducting circuits*, *Phys. Rev. Lett.* **110** (2013) 113602.
- [52] S. Felicetti, C. Sabín, I. Fuentes, L. Lamata, G. Romero and E. Solano, *Relativistic motion with superconducting qubits*, *Phys. Rev. B* **92** (2015) 064501.
- [53] Z. Huang and H. Situ, *Protection of quantum dialogue affected by quantum field*, *Quantum Information Processing* **18** (2019) .
- [54] Z. Huang and Z. He, *Deterministic secure quantum communication under vacuum fluctuation*, *The European Physical Journal D* **74** (2020) .
- [55] M.R.R. Good, A. Laponi, O. Luongo and S. Mancini, *Quantum communication through a partially reflecting accelerating mirror*, *Phys. Rev. D* **104** (2021) 105020.
- [56] S. Hengl, J. Åberg and R. Renner, *Directed quantum communication*, Tech. Rep. (2009).
- [57] R. Chatterjee, S. Gangopadhyay and A.S. Majumdar, *Violation of equivalence in an accelerating atom-mirror system in the generalized uncertainty principle framework*, *Phys. Rev. D* **104** (2021) 124001.
- [58] R. Chatterjee, S. Gangopadhyay and A. S. Majumdar, *Resonance interaction of two entangled atoms accelerating between two mirrors*, *Eur. Phys. J. D* **75** (2021) 179.
- [59] I. Akal, Y. Kusuki, N. Shiba, T. Takayanagi and Z. Wei, *Holographic moving mirrors*, *Classical and Quantum Gravity* **38** (2021) 224001.
- [60] J. Zhang and H. Yu, *Unruh effect and entanglement generation for accelerated atoms near a reflecting boundary*, *Phys. Rev. D* **75** (2007) 104014.
- [61] R. Zhou, R.O. Behunin, S.-Y. Lin and B. Hu, *Boundary effects on quantum entanglement and its dynamics in a detector-field system*, *Journal of High Energy Physics* **2013** (2013) .
- [62] S. Cheng, H. Yu and J. Hu, *Entanglement dynamics for uniformly accelerated two-level atoms in the presence of a reflecting boundary*, *Phys. Rev. D* **98** (2018) 025001.
- [63] Z. Liu, J. Zhang and H. Yu, *Entanglement harvesting in the presence of a reflecting boundary*, *Journal of High Energy Physics* **2021** (2021) .
- [64] E. Arias, T.R. de Oliveira and M. Sarandy, *The unruh quantum otto engine*, *Journal of High Energy Physics* **2018** (2018) .
- [65] F. Gray and R.B. Mann, *Scalar and fermionic unruh otto engines*, *Journal of High Energy Physics* **2018** (2018) .
- [66] H. Xu and M.-H. Yung, *Unruh quantum otto heat engine with level degeneracy*, *Physics Letters B* **801** (2020) 135201.
- [67] G.R. Kane and B.R. Majhi, *Entangled quantum unruh otto engine is more efficient*, *Physical Review D* **104** (2021) L041701.
- [68] D. Barman and B.R. Majhi, *Constructing an entangled unruh otto engine and its efficiency*, *Journal of High Energy Physics* **2022** (2022) .
- [69] S. Haroche and J.-M. Raimond, *Exploring the quantum: atoms, cavities, and photons*, Oxford university press (2006), [10.1093/acprof:oso/9780198509141.001.0001](https://doi.org/10.1093/acprof:oso/9780198509141.001.0001).
- [70] M.O. Scully, V.V. Kocharovsky, A. Belyanin, E. Fry and F. Capasso, *Enhancing acceleration radiation from ground-state atoms via cavity quantum electrodynamics*, *Phys. Rev. Lett.* **91** (2003) 243004.

- [71] A. Belyanin, V.V. Kocharovskiy, F. Capasso, E. Fry, M.S. Zubairy and M.O. Scully, *Quantum electrodynamics of accelerated atoms in free space and in cavities*, *Phys. Rev. A* **74** (2006) 023807.
- [72] E. Arias, J. Dueñas, G. Menezes and N. Svaiter, *Boundary effects on radiative processes of two entangled atoms*, *Journal of High Energy Physics* **2016** (2016) .
- [73] L. Rizzuto, *Casimir-polder interaction between an accelerated two-level system and an infinite plate*, *Physical Review A* **76** (2007) 062114.
- [74] A. Sachs, R.B. Mann and E. Martín-Martínez, *Entanglement harvesting and divergences in quadratic unruh-dewitt detector pairs*, *Physical Review D* **96** (2017) 085012.
- [75] J. Louko and V. Toussaint, *Unruh-dewitt detector's response to fermions in flat spacetimes*, *Physical Review D* **94** (2016) 064027.
- [76] S. Takagi, *Vacuum noise and stress induced by uniform accelerationhawking-unruh effect in rindler manifold of arbitrary dimension*, *Progress of Theoretical Physics Supplement* **88** (1986) 1.
- [77] D. Hümmer, E. Martín-Martínez and A. Kempf, *Renormalized unruh-dewitt particle detector models for boson and fermion fields*, *Phys. Rev. D* **93** (2016) 024019.
- [78] L. Astrakhantsev and O. Diatlyk, *Massive scalar field theory in the presence of moving mirrors*, *International Journal of Modern Physics A* **33** (2018) 1850126.
- [79] E.M. Purcell, *Spontaneous emission probabilities at radio frequencies*, in *Confined Electrons and Photons: New Physics and Applications*, E. Burstein and C. Weisbuch, eds., (Boston, MA), pp. 839–839, Springer US (1995), DOI.
- [80] L. García-Álvarez, S. Felicetti, E. Rico, E. Solano and C. Sabín, *Entanglement of superconducting qubits via acceleration radiation*, *Scientific reports* **7** (2017) 1.
- [81] Y.A. Cengel, M.A. Boles and M. Kanoğlu, *Thermodynamics: an engineering approach*, vol. 5, McGraw-hill New York (2011).
- [82] R. Balian, D. Haar and J. Gregg, *From Microphysics to Macrophysics: Methods and Applications of Statistical Physics*, no. v. 1 in Theoretical and Mathematical Physics, Springer Berlin Heidelberg (2006).
- [83] M.E. Peskin, *An introduction to quantum field theory*, CRC press (2018), [10.1201/9780429503559](https://doi.org/10.1201/9780429503559).
- [84] N.D. Birrell and P. Davies, *Quantum fields in curved space*, Cambridge university press (1984), [10.1017/CBO9780511622632](https://doi.org/10.1017/CBO9780511622632).
- [85] E. Freitag and R. Busam, *Complex Analysis*, Universitext, Springer Berlin Heidelberg (2009).
- [86] I.S. Gradshteyn, I.M. Ryzhik, D. Zwillinger and V. Moll, *Table of integrals, series, and products; 8th ed.*, Academic Press, Amsterdam (Sep, 2014), [0123849330](https://doi.org/10.123849330).
- [87] C. Ferreira and J.L. López, *Asymptotic expansions of the hurwitz–lerch zeta function*, *Journal of Mathematical Analysis and Applications* **298** (2004) 210.
- [88] K. Koźdoń, I.T. Durham and A. Dragan, *Measuring acceleration using the Purcell effect*, *Quantum* **2** (2018) 83.